ORGANOMETALLICS

pubs.acs.org/Organometallics Article

A Cationic Pt(II) Dinitrogen Adduct: Synthesis and Characterization of a CCC-aNHC Pincer Pt Complex with Abnormal *N*-Heterocyclic Carbene Donor Arms

Evans Fosu, Nghia Le, Taofiq Abdulraheem, Bruno Donnadieu, Amanda L. Patrick,* Charles Edwin Webster,* and T. Keith Hollis*

Cite This: https://doi.org/10.1021/acs.organomet.3c00411 Read Online

ACCESS | Metrics & More | Article Recommendations | Supporting Information

ABSTRACT: In contrast to the reported CCC-NHC pincer ligands that contain normal *N*-heterocyclic carbenes (NHC), herein we report an imidazole-based abnormal NHC (aNHC) pincer ligand, CCC-aNHC. The CCC-aNHC pincer Pt complex with two aNHC donors was synthesized via the *in situ* metalation and transmetalation methodology. The 1,3-phenylene(bis-2-phenyl-3-butyl imidazolium) diiodide salt was reacted with $Zr(NMe_2)_4$ to generate a CCC-aNHC pincer zirconium complex *in situ*. It was transmetalated to Pt using $[Pt(COD)Cl_2]$. Electrospray ionization of the Pt pincer complex $[(^{Bu}C^{a\text{-}i}C^{a\text{-}i}C^{Bu})\text{-}PtI]$ in acetonitrile generated an intense peak at m/z = 696.2375, which was assigned to the dinitrogen adduct $[M-I+N_2]^+$ of the cationic CCC-aNHC pincer Pt(II) complex $[(^{Bu}C^{a\text{-}i}C^{a\text{-}i}C^{Bu})Pt-N_2]^+$, representing a rare example of the platinum dinitrogen organometallic complex. The super electron-donating ability of the pincer ligands with abnormal NHC enabled the cationic CCC-aNHC pincer Pt(II) complex to selectively bind N_2 over MeCN in a first-order analysis. A collision-induced dissociation (CID) study was conducted on the N_2 and MeCN adducts, suggesting that more energy was required to dissociate N_2 than MeCN. A computational study suggested that the N_2 adduct was kinetically stable in the gas phase whereas the MeCN adduct was thermodynamically preferred. The computational results reconciled the mass spectral data experiment with an attempt to isolate the N_2 adduct. DFT computation suggested that N_2 dissociation is more challenging due to higher energy transition states, and there is a competitive pathway of N_2 tumbling within the coordination sphere of the Pt. This tumbling path is not available from the MeCN ligand due to ligand structural differences.

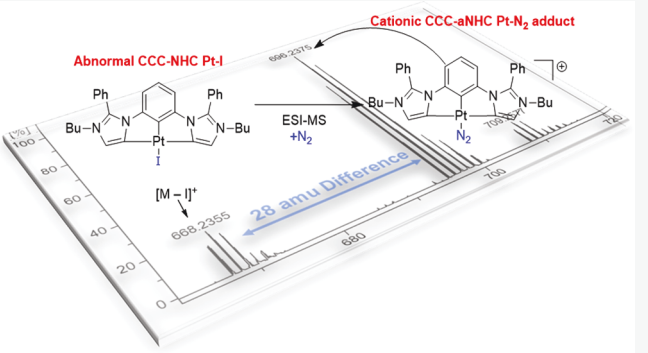

INTRODUCTION

The main challenge of ammonia (NH_3) production is the high energy demand for dinitrogen activation and dihydrogen generation.[1] The production of ammonia is important for the synthesis of fertilizers to feed the world.[2] Ammonia is also an important commodity used in the production of pharmaceuticals and cleaning agents, contributing to the advancement of modern living standards.[3] Biologically, the nitrogenase enzyme converts the N_2 into ammonia using the iron−molybdenum−sulfur protein known as the FeMo-cofactor.[4] While much of the mechanism of the operation of such N_2 fixation has been elucidated, there are still aspects of this process that remain speculative.[5] The method employed industrially to activate N_2 molecules to produce ammonia is the Haber−Bosch (HB) process.[6] Even though it is effective for producing ammonia from molecular N_2 and H_2, it requires a high energy input. The HB process requires 200−400 atm and 400−650 °C to activate dinitrogen and molecular hydrogen in the presence of heterogeneous catalysts.[7] Another major concern is that the hydrogen used for ammonia production comes from methane reforming, which produces a large volume of carbon dioxide (CO_2).[8] CO_2 contributes to the greenhouse gas effect and raises environmental concerns.[9] Therefore, less energy-consuming techniques and more environmentally friendly procedures are desired for the activation of molecular N_2 and H_2 to produce ammonia.[10] These concerns have encouraged scientific investigations in search of catalysts that might operate to activate dinitrogen and molecular hydrogen at lower temperatures and pressures.[11] Organometallic catalysts have been envisioned as a way to explore dinitrogen functionalization. These catalysts will allow the exploration of the

Received: September 25, 2023
Revised: January 5, 2024
Accepted: January 9, 2024

Chart 1. General Representations of Common Aryl-Bridged Bis-NHC Pincer Complexes[a]

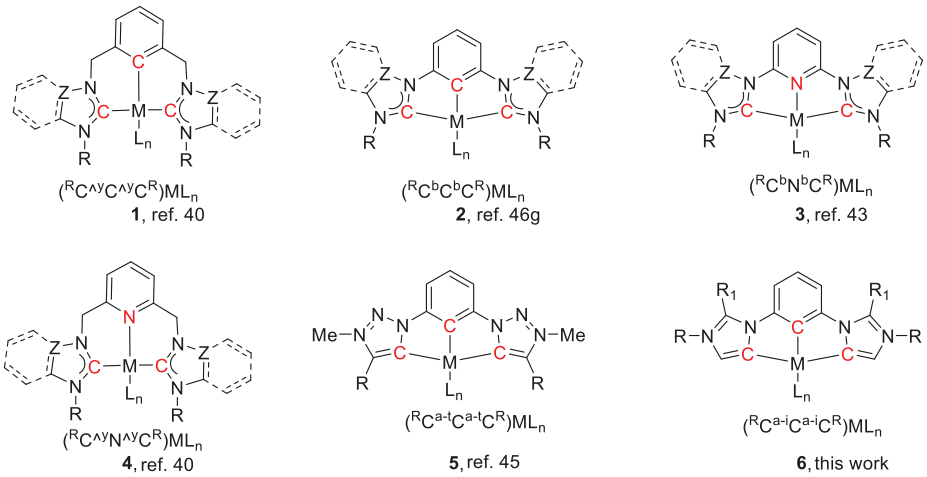

[a]For the aryl-bridged bis-NHC pincer ligands, the standard acronyms, CNC or CCC, are used to highlight the atoms bonded to the central metal. The carat (^) is used to signify a spacer that breaks conjugation and induces conformational complexity. The superscript "y" identifies imidazole-based (i), benzimidazole-based (b), or triazole-based (t) NHCs. a-i = abnormal imidazole-based NHC, a-t = abnormal triazole-based NHC, Z = CH or N, and the superscripts R, R_1= alkyl or aryl substituent. The shorthand was adapted from literature reports.[40,47g]

mechanisms to find better conditions to produce ammonia and other value-added chemicals.[12]

The report of the first ruthenium dinitrogen complex by Allen and Senoff[13] encouraged numerous research groups to study the coordination chemistry of dinitrogen complexes. Since then, many dinitrogen complexes of various metals across the periodic table have been reported. With each advancement, the importance of the ligands that surround the metal center becomes increasingly significant.[14] Group 6 dinitrogen complexes have been reported with bidentate ligands such as bis(diethylphosphino) ethane and bis-(diphenylphosphino) ethane. Molybdenum and tungsten complexes of the bidentate phosphino ligands were used as catalysts to functionalize N_2 at 20 °C to obtain 0.7 and 1.9 ammonia per Mo and W atoms, respectively.[15] Previous reports of tripodal,[16] tetrapodal,[17] and pentapodal[17a] Mo dinitrogen complexes with various proton sources functionalized N_2 to NH_3 and H_2N-NH_2.[18] Additionally, the group 4, 6, 7, 8, and 9 transition metal complexes containing amido, phosphine, and *N*-heterocyclic carbene (NHC) pincer ligands have also been reported to functionalize N_2 to ammonia under ambient conditions.[19] Organometallic complexes of group 10 metals are routinely used as homogeneous catalysts to transform organic substrates and activate small molecules to produce useful chemicals.[20] Among the group 10 organometallic complexes, only a few organonickel complexes have been characterized and demonstrated to bind N_2.[21] However, sterically hindered ligands are used to synthesize nickel N_2 complexes.[22] There have been no reported synthetic methodologies for the isolation of N_2 complexes of either platinum or palladium. No single X-ray crystal structure of N_2 organoplatinum or organopalladium complexes is yet known. A low-frequency vibrational technique has been employed to observe Pd−N_2 and Pt−N_2 bond stretching modes on the surfaces of those metals.[23] Ethylene bound to platinum metal as an organometallic complex was proposed by Zeise with many variations having been reported afterward.[24] However, there are no reports of Zeise's platinum complexes of N_2 having been isolated yet. An electrospray ionization mass spectrometry analysis of $K_2[PtCl_4]$ (Zeise's salt) solutions has been reported recently to generate ions corresponding to N_2 adducts of trichloroplatinate(II) $[PtCl_3(N_2)]^-$ species.[25] Ions such as $[Pt(NH_3)_2(N_2)Cl]^+$, $[Pt(NH_3)_2(N_2)OH]^+$, and $[PtCl_3N_2]^-$ were reported by Cui and co-workers when studying the hydrolysis of cisplatin using a Fourier transform ion cyclotron resonance mass spectrometry technique.[26] Furthermore, an electrospray ionization of group 10 complexes of phenanthroline was reported to generate inorganic fragments $[(phen)Pt]^+$ of N_2, O_2, and H_2O in the gas phase.[27] These reports stimulated us to speculate that having strong electron donating ligand(s) around the Pt cation may lead to the isolation and characterization of Pt dinitrogen complexes. One of the strongest electron donor ligands in organometallic chemistry is the abnormal NHC ligand.[28]

NHCs have been used as ancillary ligands for over 50 years and are considered to be stronger electron donors than phosphines and pyridines.[29] Imidazole-2-ylidene and its derivatives are widely explored in the field of NHC chemistry.[30,31] NHC ligands have been reported to be more air- and moisture-stable than phosphine ligands. The NHCs can be classified as normal (nNHC) and abnormal (aNHC) or mesoionic (MIC),[38] which are based on their binding mode to the metal ions. The most explored among these categories are the nNHCs where the carbene is featured on the C2 position of 1,2,4-triazolium or imidazolium ligands.[32] However, the aNHCs have gained considerable attention because of their stronger electron donating power.[33,34] The aNHC ligands feature the carbene carbon at the C4 or C5 position on the imidazolium or 1,2,3-triazoliun ligands instead of the C2 position.[35] Crabtree and co-workers described an aNHC-metal complex in 2001, but the stable unmasked aNHC was reported in 2009 by Bertrand et al. Tolman electronic parameters and quantum chemical calculations predicted a stronger electron donating ability of aNHCs versus the corresponding nNHCs.[36] The exceptional donating ability of the aNHC ligands has made them crucial in the design and synthesis of multidentate ligands,[37] in particular, pincer architectures where NHCs serve as terminal donors.[38] Also, the use of aNHCs has emerged as a new strategy to synthesize high valence metal complexes.[38b] To date, a C2-deprotonation of imidazolium salts has been the

https://doi.org/10.1021/acs.organomet.3c00411
Organometallics XXXX, XXX, XXX−XXX

Scheme 1. Synthesis of the CCC-aNHC Pt(II) Pincer Complex 9 from C2 Arylated 1,3-Bis(*N*-butyl-2-phenyl imidazolium)benzene Diiodide 8

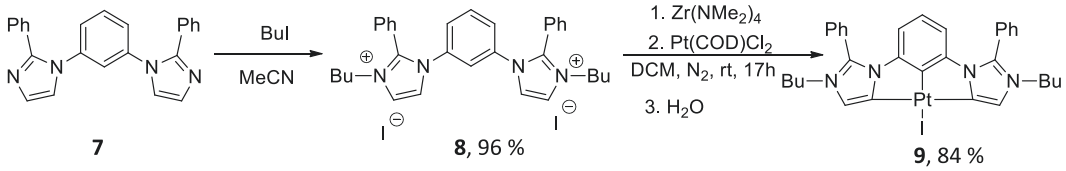

most reliable approach for the synthesis of NHC pincer complexes.[39] For instance, the report of monoanionic CCC-NHC pincer complexes **1**[40] and **2**[41] and neutral CNC-NHC pincer complexes **3**[42] and **4**[43] (Chart 1) relied on C2-deprotonation of the azolium salts because of the higher acidity of the C2 protons.[44] Due to the weaker acidity of C4 and C5 protons versus the C2 proton of the imidazolium salts, the most frequently synthesized aNHC pincer complexes are the 1,2,3-triazole based complexes **5**.[45] The monoanionic 1,2,3-triazole based aNHC pincer ligands have been reported to stabilize Pd(IV) species that are particularly considered as transient intermediates in Pd catalyzed reactions.[46] Our group has been developing normal CCC-NHC pincer complexes **2** employing $Zr(NMe_2)_4$ as a base and a metal source from phenylene bridged azolium proligands.[47] The modulation of the phenylene bridged NHC pincer ligands for the synthesis of abnormal CCC-NHC pincer complexes has been one research interest of our group.[48] Even though CCC-NHC pincer complexes of palladium and platinum have been reported by our group and others, none have been reported to bind N_2.[49] Herein, we report a gas phase dinitrogen adduct of an imidazole-based CCC-aNHC pincer platinum complex **6** (Chart 1) employing a phenylene bridged C2 arylated bis(imidazolium) ligand.

RESULTS AND DISCUSSION

Compounds 1,3-bis(2-phenylimidazole) benzene **7** and 1,3-bis(2-phenylimidazolium) benzene diiodide salt **8** $[(^{Bu}C^{a\text{-}i}C^{a\text{-}i}C^{Bu})(H)_3][I]_2$ (Scheme 1) were synthesized by a slight modification of procedures from the literature.[47i]

The CCC-aNHC pincer Pt complex **9** was synthesized by *in situ* metalation of **8** with $Zr(NMe_2)_4$ and subsequently transmetalated to Pt using $Pt(COD)Cl_2$. The addition of $Zr(NMe_2)_4$ to a solution of **8** in methylene chloride gave a colorless solution. The ^{1}H NMR spectrum of the solution revealed the absence of the singlet phenylene proton at 8.45 ppm and the C5 imidazolium doublet at 7.98 ppm (see SI Figure S5). The spectrum showed multiple products within a 10 min reaction time but resolved to a symmetrical or a single product after 17 h. The triplet signal corresponding to the methylene group adjacent to the imidazolium nitrogen appeared at 3.85 ppm for the Zr adduct in DCM. The singlet C4 protons on the imidazolium arms shifted from 7.77 ppm downfield to 7.39 ppm, and the triplet on the phenylene bridging the two imidazolium arms appeared at 6.59 ppm (see SI Figure S5). The transmetalation reaction from the *in situ* generated zirconium complex to Pt using $Pt(COD)Cl_2$ gave a solution of intense yellow color. The ^{1}H NMR spectrum of the solution showed a complete quantitative transmetalation to the Pt within 20 min. The singlet imidazolium protons at 7.39 ppm in the *in situ* generated Zr complex shifted to 7.13 ppm. The C4 proton on the imidazolium arms at a chemical shift of 7.13 ppm coupled to the Pt with satellite peaks that were clearly observable ($^3J_{Pt-H}$ = 5 Hz, im-H) in the ^{1}H NMR spectrum. After workup, the CCC-aNHC Pt(II) iodide complex **9**, $[(^{Bu}C^{a\text{-}i}C^{a\text{-}i}C^{Bu})PtI]$, was obtained as the product according to spectroscopic studies (^{1}H, ^{13}C NMR, and X-ray spectroscopies). To establish the purity and unequivocally identify the halogen of the bulk material of complex **9**, the powdered and crystalline samples were subjected to elemental analysis. The elemental analyses were within the acceptable range for complex **9**. In 2013, the normal CCC-NHC Pt chloride pincer complex was reported based on the same methodology using bis(3′-trimethylsilylmethylbenzimidazol-1′-yl)benzene diiodide salt.[50] Probably, this is owed to the fact that the trimethylsilylmethyl group is sterically bulky or the Pt center is more Lewis acidic. In contrast, the CCC-aNHC pincer Pt complex conclusively binds iodide, the only product observed. The formation of the platinum iodide product suggests that the auxiliary halide on the metal center originated from the salt **8**. Also, the formation of the iodide product is due to the fact that the strong electron-donating ability of the aNHC arms of the ligand and strong anionic aryl group will in principle stabilize the soft Lewis acid Pt(II) center. The soft acid Pt(II) preferentially binds to the soft iodide ion to give quantitative formation of the iodide adduct. Crystals suitable for X-ray crystallography were obtained from slow vapor diffusion of diethyl ether into a saturated solution of dichloromethane. The diffraction study confirmed the molecular structure of the Pt(II) pincer complex **9**. The complex exhibited a distorted square-planar configuration as expected for d^8 four-coordinate transition-metal compounds of group 10. An ORTEP plot of the molecular structure of complex **9** is presented in Figure 1. The bond lengths of the Pt(II) pincer complex are consistent with the previously reported NHC pincer complexes.[51] The $Pt-C_{carbene}$ bond length in the complex was determined to be 2.019(8) Å, and a bond length of 1.923(9) Å was observed for the $Pt-C_{aryl}$. There are no significant changes in bond lengths between the CCC-aNHC pincer Pt(II) complex **9** and the reported normal CCC-NHC pincer Pt complexes[52] where chloride and bromide were the auxiliary anions on the Pt.

ESI-MS Analysis of CCC-aNHC Pt Pincer Complex 9 and the Observation of the Cationic Platinum Dinitrogen Adduct $[(^{Bu}C^{a\text{-}i}C^{a\text{-}i}C^{Bu})Pt-N_2]^+$. An electrospray ionization mass spectrometry (ESI-MS) analysis was performed on complex **9**. The spectrum is presented in Figure 2. There were three distinct peaks in the mass spectrum with Pt isotope envelopes of six in each single peak. The envelopes of peaks represent the isotope distribution of Pt.[53] Among those three peaks was a peak at m/z = 668, A, which corresponds to the expected dehalogenated adduct $[(^{Bu}C^{a\text{-}i}C^{a\text{-}i}C^{Bu})Pt]^+$, **10**. In the spectrum was another peak, B, observed at m/z = 696.2375 which corresponds to the adduct **10** bound to a species with a mass of 28 amu (structure **11**).

In fact, in this full-scan spectrum, the m/z = 696.2375 was the most intense peak in the spectrum. Ethylene, dinitrogen,

https://doi.org/10.1021/acs.organomet.3c00411
Organometallics XXXX, XXX, XXX−XXX

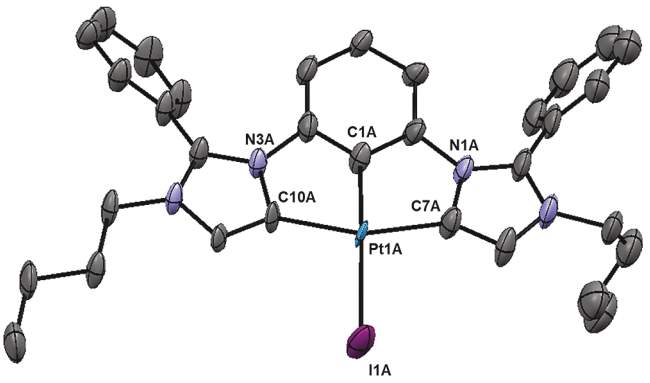

Figure 1. ORTEP diagram of abnormal platinum iodide complex **9**, [($^{Bu}C^{a-i}C^{a-i}C^{Bu}$)PtI]. Hydrogen atoms are omitted for clarity. The thermal ellipsoids are shown at 95% probability. Bond distances (Å): Pt1A−C1A = 1.923(9); Pt1A−C10A = 2.019(8); Pt1A−C7A = 2.046(8); Pt1A−I1A = 2.6845(7); N3A−C10A = 1.405(12); N1A−C7A = 1.428(11). Bond angles (deg): C1A−Pt1A−C10A = 79.6(4); C1A−Pt1A−C7A = 81.0(3); C10A−Pt1A−C7A = 160.6(4); C1A−Pt1A−I1A = 175.7(3); C10A−Pt1A−I1A = 96.2(3); C7A−Pt1A−I1A = 103.1(2). C11A−C10A−N3A = 103.8(7); N1A−C7A−Pt1A = 110.7(6).

and carbon monoxide molecules all have a nominal mass of 28 amu, and any one of them could, in principle, act as a ligand on the dehalogenated fragment of the cationic complex [($^{Bu}C^{a-i}C^{a-i}C^{Bu}$)Pt]$^+$, **10**. Given that nitrogen (N_2) is abundant in the atmosphere and is used within the mass spectrometer, it was the likely candidate. Further, the average error calculated for all of the isotope envelopes in the peaks (Figure 3) for the hypothetical carbon monoxide complex [($^{Bu}C^{a-i}C^{a-i}C^{Bu}$)Pt-CO]$^+$, **14**, and the hypothetical ethylene complex [($^{Bu}C^{a-i}C^{a-i}C^{Bu}$)Pt−$C_2H_4$]$^+$, **15**, shows that the individual isotopic peaks of complexes **14** and **15** are off by 9.9 and 41.6 ppm (calculated mass for the carbon monoxide bound complex, **14**, was 696.2299 amu and that of the ethylene bound complex, **15**, was 696.2666 amu), whereas the N_2 bound complex [($^{Bu}C^{a-i}C^{a-i}C^{Bu}$)Pt−$N_2$]$^+$, **13**, was off by only 5.5 ppm on average. Thus, the most intense peak was assigned to the formation of the cationic N_2 complex **13** (calculated m/z = 696.2414).

Since acetonitrile was used as a solvent for the ESI-MS analysis of complex **9**, the most intense peak was expected to be the MeCN coordinated adduct **12**, but it turned out to be the least intense peak found relative to complexes **10** and **11**. The MeCN coordinated complex **12** was observed at m/z = 709 in the mass spectrum.

Comparison between the Normal and Abnormal CCC-NHC Pincer Platinum Complexes. The unexpected coordination of the N_2 to the dehalogenated adduct of complex **9** prompted us to revisit the normal CCC-NHC Pt(II) chloride pincer complex (**16**, Chart 2) previously reported by our group[52] to perform ESI-MS analysis again. Structurally, the normal CCC-NHC pincer Pt complex **16** features the carbenes on the C2 carbon atoms, and the carbene carbons are in between two nitrogen atoms. On the other hand, the CCC-aNHC Pt(II) iodide complex (**9**, Chart 2) has the carbenes featured on the C5 carbon atoms. The C5 carbons are bonded to adjacent sp^2 carbon atoms instead of electron-withdrawing nitrogen atoms. The weaker electronegative carbon atoms make the abnormal carbenes more electron efficient in complex **9** than those of **16**.

The ESI-MS analysis of complex **16** gave similar peaks in the mass spectrum as previously reported. A solution of complex **9** and complex **16** was mixed and subjected to mass analysis. The mass spectrum showed four distinct peaks as shown in Figure 4. A peak was observed at m/z = 516, which corresponds to the cationic Pt(II) adduct **17**. The remaining peaks in the mass spectrum were similar peaks observed for the analysis of complex **9** (Figure 2). The [($^{Bu}C^{a-i}C^{a-i}C^{Bu}$)Pt−$N_2$]$^+$ adduct **13** showed the most intense peak, as observed before. However, no N_2 adduct was observed for the cationic adduct of complex **16**. If it had been present, the cationic N_2 Pt(II) adduct would

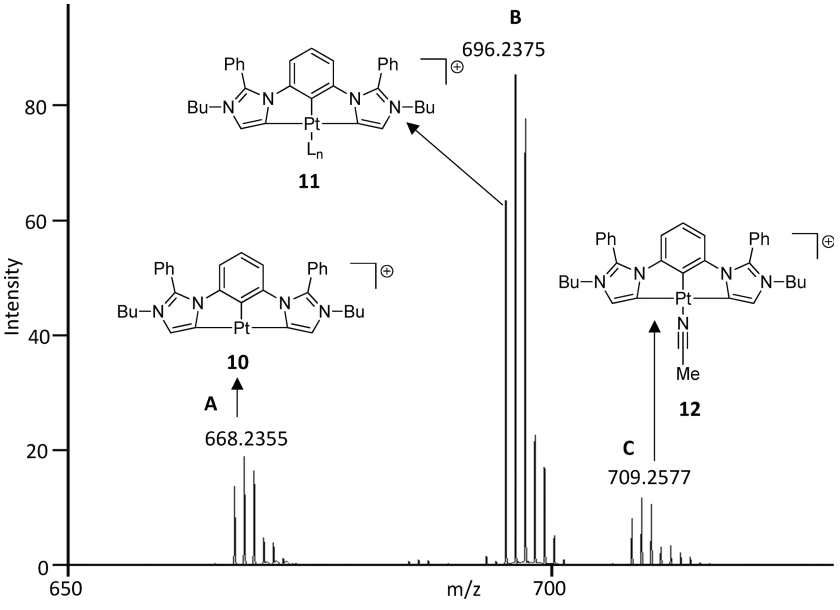

Figure 2. Positive-mode ESI-MS spectrum of the CCC-aNHC Pt(II) iodide pincer complex [($^{Bu}C^{a-i}C^{a-i}C^{Bu}$)PtI] (**9**) in MeCN. (A) [M−I]$^+$ with the mass selection of m/z = 668.2355, (B) [M−I + L_n]$^+$ with the molecular formula [($^{Bu}C^{a-i}C^{a-i}C^{Bu}$)Pt + L_n]$^+$ and m/z = 696.2375 readily formed in the gas phase, (C) [M−I+MeCN]$^+$ with a mass of m/z = 709.2577. L_n = N_2, CO, and C_2H_4.

https://doi.org/10.1021/acs.organomet.3c00411
Organometallics XXXX, XXX, XXX−XXX

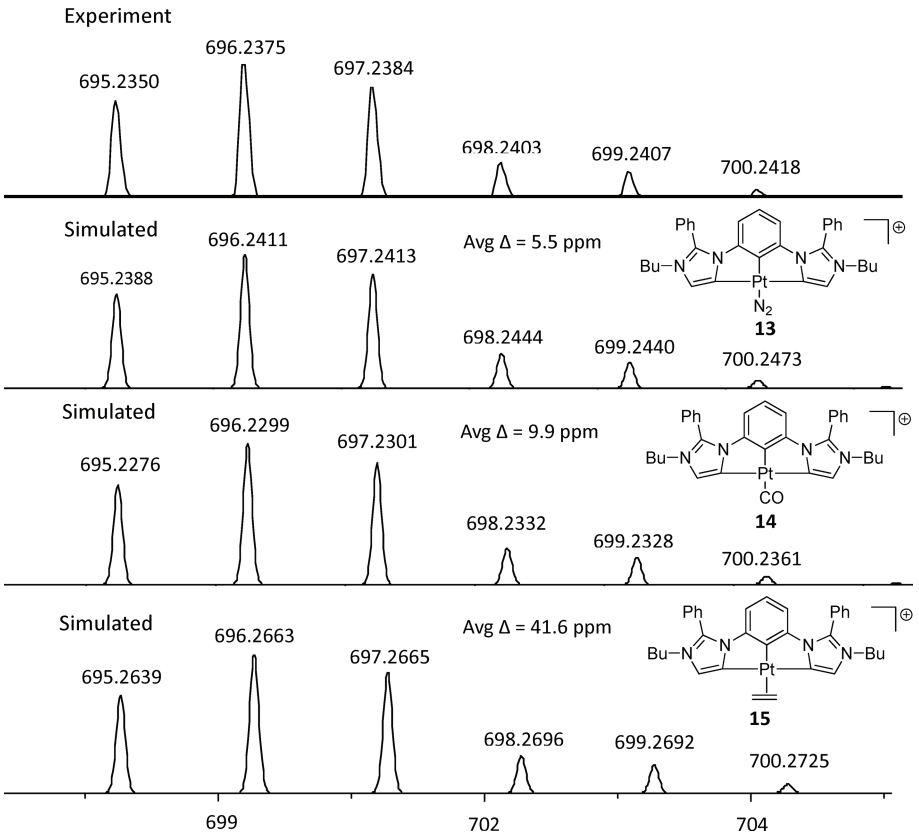

Figure 3. Simulated patterns of the dinitrogen bound adduct $[(^{Bu}C^{a\text{-}i}C^{a\text{-}i}C^{Bu})Pt{-}N_2]^+$ (**13**), carbon monoxide bound adduct $[(^{Bu}C^{a\text{-}i}C^{a\text{-}i}C^{Bu})Pt\text{-}CO]^+$ (**14**), and ethylene bound adduct $[(^{Bu}C^{a\text{-}i}C^{a\text{-}i}C^{Bu})Pt{-}C_2H_4]^+$ (**15**) to the dehalogenated adduct of the Pt(II) complex. The Δppm is the average of all the isotope peaks.

Chart 2. Normal CCC-NHC Pt Pincer Complex 16 versus Abnormal CCC-NHC Pincer Pt(II) Complex 9[a]

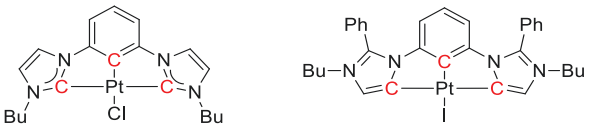

16 **9**

[a]For more about the normal of CCC-NHC see ref 47g.

be expected to appear at m/z = 544 (indicated as **17** + N_2 arrow with an asterisk in Figure 4). No peak was observed at that position. Also, no MeCN adduct of the cationic complex **17** was observed (calculated to be 557.1992 amu). This observation confirms the uniqueness of the CCC-aNHC ligand in the Pt(II) pincer complex **9**.

Where is the N_2 Coming From? To further investigate the source of the dinitrogen molecule, the operating gas of the mass spectrometer was switched from N_2 gas to Ar gas without altering any other acquisition parameters. Using Ar gas, the mass spectrum still showed the most intense peak at m/z = 696 (Figure S14), which corresponds to the N_2 coordinated to the cationic Pt(II) complex, **13**. This observation also suggested that the acetonitrile used as a solvent was saturated with N_2 from the atmosphere, and that allowed the N_2 adduct **13** to be formed.

To test whether the acetonitrile solvent was the source of N_2, a sample was degassed by the freeze−pump−thaw method. Afterward, the solution was subjected to mass analysis by ESI-MS under Ar as a carrier gas. In this case, the peak at 696 decreased significantly in intensity, as may be seen in Figure 5. The peak at m/z = 668 which represented the cationic adduct **10** was the most intense peak instead (compare Figure 5 versus Figure 2). Coincidentally, two new extraneous peaks due to adventitious water were observed (m/z = 684 and 702) as confirmed by exact mass analysis. They are assigned as the oxo species **18** and the hydroxy species **19** (see SI Figures S16 and S17 and discussion therein). Thus, the N_2 saturated MeCN solvent was identified as the source of N_2.

Collision-Induced Dissociation (CID) Studies of $[(^{Bu}C^{a\text{-}i}C^{a\text{-}i}C^{Bu})PtI]$. Based on the relative intensities of the dinitrogen versus the acetonitrile adducts in the ESI experiments, a first-order analysis could be that the N_2 coordinates cationic $[(^{Bu}C^{a\text{-}i}C^{a\text{-}i}C^{Bu})\text{-}Pt\text{-}N_2]^+$ complex **13** more stably than the MeCN coordinated adduct **12** under the ESI-MS conditions. To investigate this possibility, energy-resolved collision-induced dissociation mass spectrometry (CID-MS) studies were conducted using an ion trap mass spectrometer. Energy-resolved CID-MS has been used to predict the relative strength or stability of the chemical bonds in compounds,[25a] especially when they have comparable degrees of freedom and masses. It is expected that the weaker bond would cleave at lower collision energy than a stronger bond.[54] The full scan spectrum from the ion trap mass spectrometer showed peaks corresponding to $[(^{Bu}C^{a\text{-}i}C^{a\text{-}i}C^{Bu})Pt{-}N_2]^+$ adduct **13** at m/z = 696, $[(^{Bu}C^{a\text{-}i}C^{a\text{-}i}C^{Bu})Pt{-}NCMe]^+$ adduct **12** at m/z = 709, and $[(^{Bu}C^{a\text{-}i}C^{a\text{-}i}C^{Bu})Pt]^+$ complex **10** at m/z = 668. Each of the two adducts was, in turn, mass isolated with an isolation width of 3.0 amu and subjected to various collision energies. Upon CID, both adducts generated a major fragment ion at m/z = 668 due

https://doi.org/10.1021/acs.organomet.3c00411
Organometallics XXXX, XXX, XXX−XXX

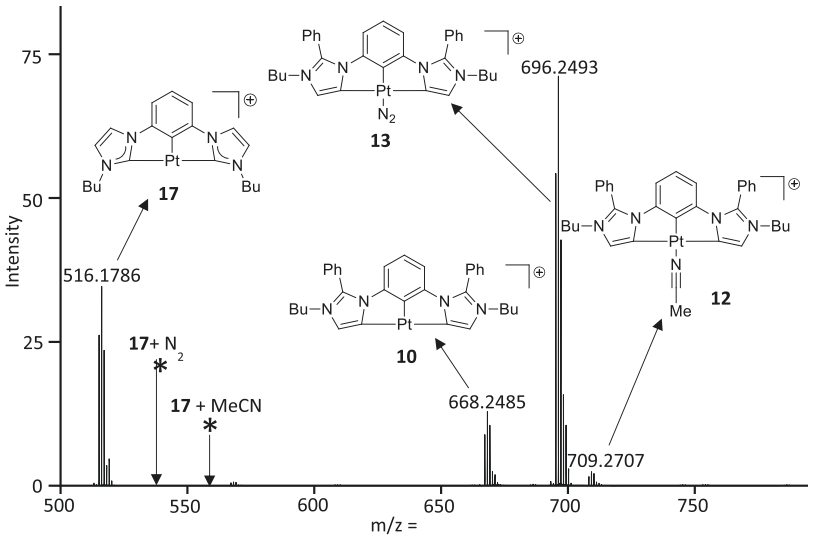

Figure 4. Positive-mode ESI-MS spectrum of complexes **9** and **16** combined in acetonitrile solvent. The arrows with the asterisk indicate where the positions of the normal CCC-NHC Pt(II) complex **17** adducts with N_2 or MeCN would have been.

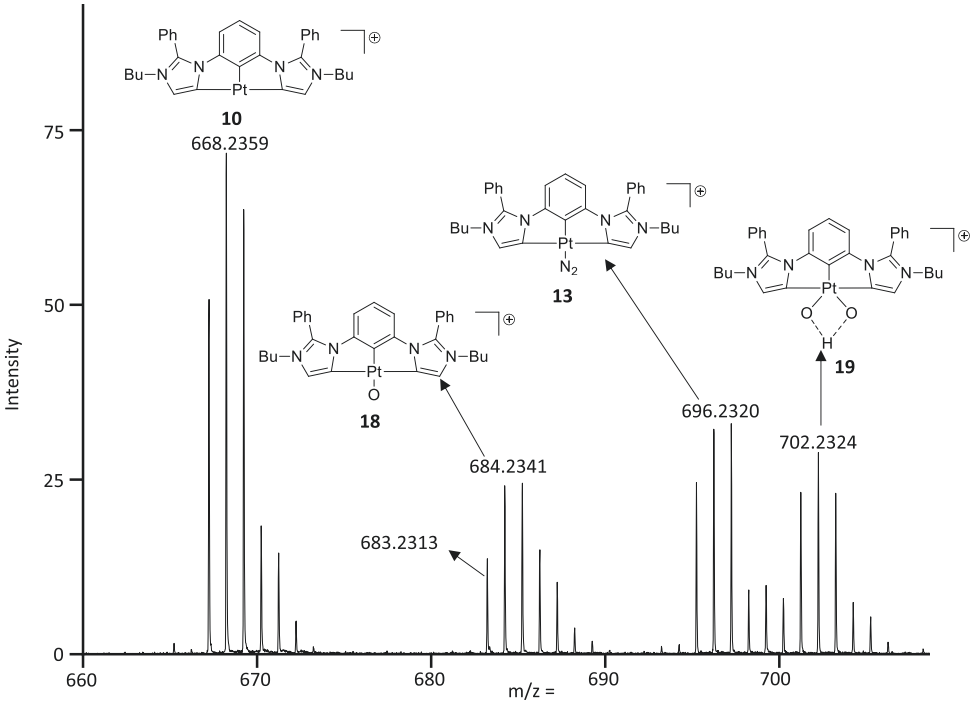

Figure 5. Positive-mode ESI mass spectrum of a solution of complex **9** in acetonitrile degassed with Ar gas. The intensity of the $[(^{Bu}C^{a\text{-}i}C^{a\text{-}i}C^{Bu})Pt{-}N_2]^+$ peak decreased drastically under the Ar environment. The peaks at m/z = 684.2341 and 702.2324 correspond to $[(^{Bu}C^{a\text{-}i}C^{a\text{-}i}C^{Bu})Pt(O)]^+$ and $[(^{Bu}C^{a\text{-}i}C^{a\text{-}i}C^{Bu})Pt(O)(OH)]^+$ adducts.

to the loss of N_2 (−28 amu) or a MeCN (−41 amu) ligand. Therefore, only the precursor ion and the m/z = 668 fragment ions were considered in the calculation of the percentage yield (Figure 6).

In the energy-resolved CID-MS, a sharp decay in precursor intensities (and a corresponding increase in product ion intensities) occurred at normalized collision energies (NCE) of 13 and 16 for N_2 and MeCN adducts, respectively. The N_2 complex achieved 50% depletion at NCE 18.4, whereas the MeCN complex achieved it at a lower NCE of 14.3. The experiment was conducted two more times (see SI Figures S19−S25 for more information), and the curve was reproducible with similar 50% reduction values: 50% depletion of N_2 complex at NCE 18.6 ± 0.6 and 50% depletion of the MeCN complex at NCE 14.4 ± 0.6. The higher NCE of the N_2 adduct indicates that the $[(^{Bu}C^{a\text{-}i}C^{a\text{-}i}C^{Bu})Pt\text{-}N_2]^+$, **13**, required more energy input to dissociate on the time scale of the CID-MS experiment. However, the kinetic versus thermodynamic implications of this observation cannot be readily disentangled from this experimental data alone. Thus, we turned to a computational evaluation of the cationic CCC-NHC pincer Pt complexes.

Computational Results. To gain further insight into the stability of N_2 and MeCN coordination to the cationic CCC-aNHC Pt(II) pincer complexes, density functional theory studies (DFT) were performed. Three cationic CCC-NHC

https://doi.org/10.1021/acs.organomet.3c00411
Organometallics XXXX, XXX, XXX−XXX

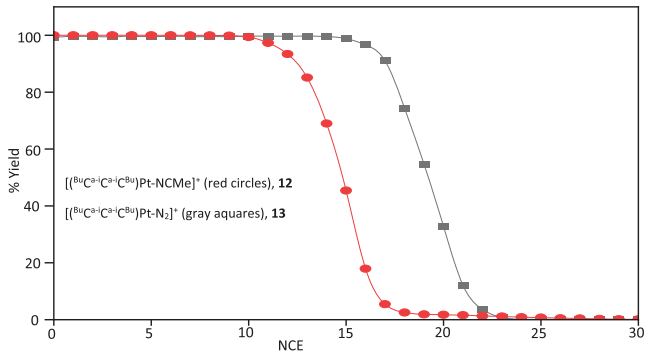

Figure 6. A representative energy-resolved CID-MS curve of the dinitrogen adduct, $[(^{Bu}C^{a\text{-}i}C^{a\text{-}i}C^{Bu})Pt{-}N_2]^+$ (**13**; gray square), and the acetonitrile adduct, $[(^{Bu}C^{a\text{-}i}C^{a\text{-}i}C^{Bu})Pt{-}NCMe]^+$ (**12**) complex (red circle).

Pt(II) pincer complexes **11**, **20**, and **21** were studied to understand (Figure 7) how the ligand architectures affect the

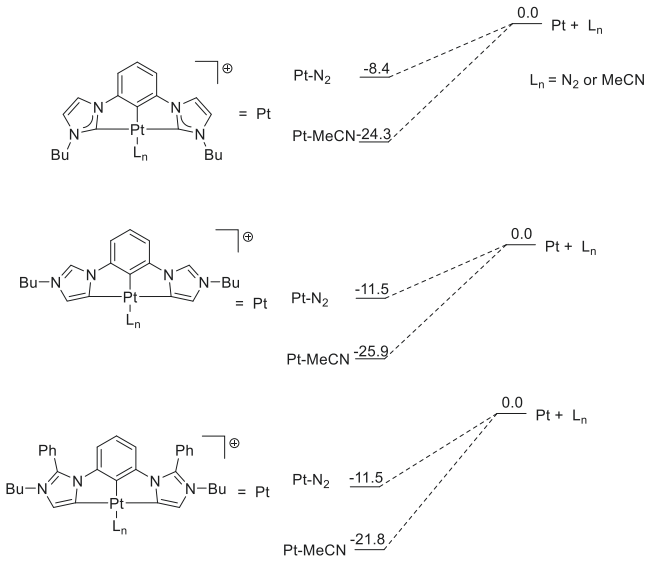

Figure 7. Gas-phase calculations of the association of the dinitrogen and acetonitrile ligands to the cationic CCC-NHC Pt(II) complexes. All energies are reported in kcal/mol.

electronic structure of the Pt metal center. The phenyl substituents on the imidazolium arms on the CCC-aNHC pincer Pt complex **11** were replaced with hydrogen atoms to understand the effect of the substituents on the formation of the $Pt{-}N_2$ adduct. The bond dissociation energy with small molecules such as N_2 provided insight into the catalytic potential and stability of important intermediates. As depicted in Figure 7, the study showed similar trends in energies between the three pincer complexes **11**, **20**, and **21**. The coordination of MeCN to the cationic CCC-NHC Pt(II) complex **20** is thermodynamically more stable than the N_2 coordination by 15.9 kcal/mol. The association of N_2 to complex **21** is thermodynamically more stable than complex **20** by 3.1 kcal/mol. The substitution of the hydrogen atoms with the phenyl substituents in complex **11** decreased the stability of the MeCN bound complex **21** by 4.1 kcal/mol. However, the substitution of the hydrogen atoms with the phenyl substituents in complex **11** did not change the stability trends of the N_2 bound complex **21**.

The N_2 ligand was computed to have the weakest coordination to the cationic Pt pincer complexes **11**, **20**, and **21** with association energies of −11.5, −8.4, and −11.5 kcal/mol, respectively. The phenyl (Ph) substituents in the pincer complex **11** did not change the trends in energies. Hou and co-workers found that back bonding mostly contributes to the coordination energy of the N_2 ligand in anionic complex $[PtCl_3N_2]^-$. For the cationic $[(^{Bu}C^{a\text{-}i}C^{a\text{-}i}C^{Bu})Pt{-}N_2]^+$, **13**, scenario, weaker π back bonding and stronger σ donation were expected. However, stronger bonds were observed in the cationic Pt complexes **11** and **21**. The stronger bonds suggest that the CCC-aNHC ligands donated electrons to the Pt metal, causing it to be electron-rich to create stronger bonds to the auxiliary ligands, especially in the high contribution of π back bonding character with the N_2 ligand. The CID data indicated that the N_2 ligand binds the cationic Pt(II) adduct more strongly than the MeCN ligand. The CID observations can be understood since normalized collision energies are not bond strength measurements in the thermodynamic sense but are a kinetically controlled process, rather.[54]

To compare the kinetic dissociation process between the cationic $[(^{Bu}C^{a\text{-}i}C^{a\text{-}i}C^{Bu})Pt{-}N_2]^+$, **13**, and $[(^{Bu}C^{a\text{-}i}C^{a\text{-}i}C^{Bu})Pt{-}NCMe]^+$, **12**, complexes, simplified model complexes were used. The *n*-butyl (Bu) and phenyl (Ph) groups in the abnormal pincer ligand were replaced by methyl (Me) and hydrogen (H) atoms, respectively, to minimize the effect of conformers and to speed up the calculations.

The data in Figure 8 show N_2 and MeCN association and dissociation pathways in CCC-aNHC Pt pincer complexes. The cationic N_2 coordinated complexes **22-g** and **23-g** ("g" is to indicates the gas phase calculation) were computed to have an energy of 87.8 kcal/mol in the gas phase. The complexes **22-g** and **23-g** originated from the dissociation of N_2 from $[(^{Me}C^{a\text{-}i}C^{a\text{-}i}C^{Me})Pt{-}N_2]^+$ through transition state complex **TS-2-g**. The N_2 ligand was found to tumble on the **TS-2-g** complex at the transition state. This tumbling behavior gave rise to a lower energy (4.3 kcal/mol) side-on activated complex **TS-1-g**. These activated complexes led to the side-on complex **23-g** and end-on complex **24-g** at the local minima where the nitrogen atoms N1 (blue) and N2 (red) swapped positions. The end-on coordination of N_2 to the cationic complex **23-g** was computed to have a relative energy of 87.8 kcal/mol, whereas the side-on isomer **24-g** gave an energy of 99.7 kcal/mol. Thermodynamically, the end-on isomer **24-g** is relatively more stable by 11.9 kcal/mol than the side-on isomer **23-g**. Also, the ligandless cationic complex **25-g** was computed to have an energy of 99.1 kcal/mol at the local minima. The CCC-aNHC Pt chloride pincer complex **26-g** was also considered in the modeling. The dissociation of the chloride ligand from complex **26-g** and the formation of MeCN complex **27-g** is thermodynamically favored by 12.5 kcal/mol compared to the more stable end-on N_2 bound complex **23-g**.

Moreover, it should be considered that the dissociation of the N_2 ligand from complex **22-g** through transition state **TS-2-g** is kinetically more energy-intensive by 5.3 kcal/mol than the dissociation of the MeCN ligand from complex **27-g** through transition state **TS-3-g** in the gas phase. The higher energy barrier of the $Pt{-}N_2$ adduct **TS-2-g** explains why, in the CID experiment, the cationic $[(^{Bu}C^{a\text{-}i}C^{a\text{-}i}C^{Bu})Pt{-}N_2]^+$ adduct, **13** required higher energy to dissociate than the cationic $[(^{Bu}C^{a\text{-}i}C^{a\text{-}i}C^{Bu})Pt{-}NCMe]^+$ adduct, **12**. These gas phase data (CID and computations) indicate that the $Pt{-}N_2$ adduct **TS-2-g** has kinetic stability versus the acetonitrile adduct **TS-3-g**.

https://doi.org/10.1021/acs.organomet.3c00411
Organometallics XXXX, XXX, XXX−XXX

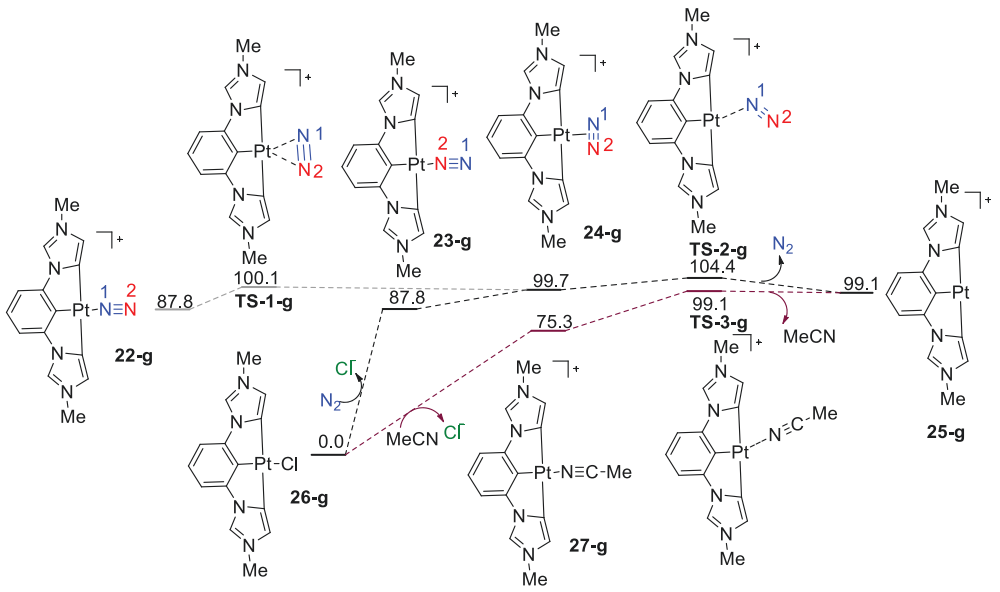

Figure 8. Gas phase calculations of $[(^{Me}C^{a\text{-}i}C^{a\text{-}i}C^{Me})Pt{-}N_2]^+$ and $[(^{Me}C^{a\text{-}i}C^{a\text{-}i}C^{Me})Pt{-}NCMe]^+$ at the PBE1PBE/BS1 level of theory. Gibbs free energy profile (kcal/mol) is presented. The "g" attached to the labeling numbers means that the complexes were computed in the gas phase. The numerical 1 and 2 on the N atom show that N swaps positions along the pathways.

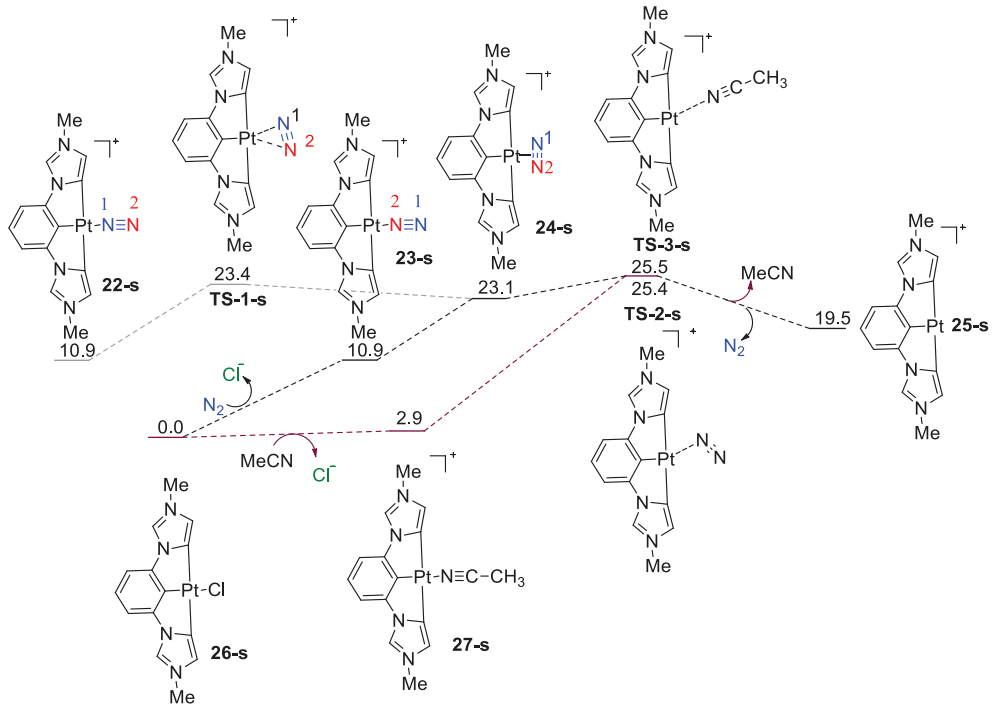

Figure 9. Solvated calculations of $[(^{Me}C^{a\text{-}i}C^{a\text{-}i}C^{Me})Pt{-}N_2]^+$ and $[(^{Me}C^{a\text{-}i}C^{a\text{-}i}C^{Me})Pt{-}NCMe]^+$ at the SMD(MeCN)//PBE1PBE/BS1 level of theory. The Gibbs free energy profile (kcal/mol) is presented. The "s" attached to the labeling numbers means the solvent was factored into the computation of the complexes. The numerical 1 and 2 on the N atom show that N swaps positions along the pathways.

When these results were noted, extensive efforts were expended to attempt to isolate the observed $Pt{-}N_2$ adduct, to no avail.

As a next step, the computational results were recalculated using an implicit solvent model to evaluate the impact of solvent on these stabilities, and the results are illustrated in Figure 9. The solvent used for the calculation was acetonitrile. The MeCN remains a better ligand than the N_2 in the case of thermodynamic sense. The formation of complex **27-s** ("s" indicates solvent was considered in the calculation) is still thermodynamically more favored by 8.0 kcal/mol over the N_2 bound complex **23-s**. The thermodynamic stability trends do not change by the incorporation of solvent into the calculations. The energy barriers of **TS-2-s** and **TS-3-s** for the dissociation of N_2 and MeCN ligands from the Pt center were computed to be 25.4 and 25.5 kcal/mol, respectively. The similarity in energies means that the acetonitrile solvent eliminated the kinetic stability observed in the gas phase calculations presented in Figure 8. These are the highest points and are therefore assigned as the rate-determining steps. The

https://doi.org/10.1021/acs.organomet.3c00411
Organometallics XXXX, XXX, XXX−XXX

closeness in activation barriers of **TS-2-s** and **TS-3-s** means that the dehalogenation of the CCC-aNHC Pt halide complexes in acetonitrile would lead to the more stable MeCN bound complexes. The computations suggest that the synthesis and isolation of the cationic CCC-aNHC Pt N_2 pincer complex, which is a kinetic product, could be more challenging compared to the CCC-aNHC Pt MeCN complex, which is a thermodynamic adduct. The higher energy barrier emphasizes why we have not been able to synthesize the cationic Pt N_2 complex upon numerous attempts. In terms of geometry, the computed transition state **TS-3-s** is connected to κ^1 MeCN, while **TS-2-s** is connected to the side-on κ^2 N_2 ligand in **24-s**. The κ^2 MeCN bound complex could not be located.

To verify the results of DFT, single point calculation with domain-based local pair natural orbital implemented on couple cluster method DLPNO−CCSD(T) was performed at def2-QZVPP basis set. If considering DLPNO-CCSD(T)/BS2/PBE0-D3/BS1 results as the standard reference, the PBE0-D3/BS1 calculation tends to underestimate the thermodynamic and kinetic values (Table S5) but shows excellent correlation (R^2 = 0.98) in the linear regression (Figure S28).

The evaluation of the kinetic dissociation process between the cationic $[(^{Me}C^{a\text{-}i}C^{a\text{-}i}C^{Me})Pt{-}N_2]^+$ and $[(^{Me}C^{a\text{-}i}C^{a\text{-}i}C^{Me})Pt{-}NCMe]^+$ complexes was also computed at the SMD-(MeCN)//PBE1PBE/BS1 level of theory. The barrier for the dissociation of the MeCN ligand from the Pt pincer complex was higher than that of the dissociation of the N_2 ligand (Figure S29). However, the energy difference is very small ($\Delta\Delta^{\ddagger}G^{\circ}$ = 1.2 kcal/mol), and no significant inferences could be drawn out of it. Structurally, the N_2 ligand is perpendicular in the plane of the pincer complex due to the steric effect of the two alkyl groups in the imidazolium arms. The two nitrogen atoms in the $[(^{Me}C^{a\text{-}i}C^{a\text{-}i}C^{Me})Pt{-}N_2]^+$ complex are horizontal to the plane of the pincer (Figure S27).

CONCLUSIONS

A new CCC-aNHC Pt(II) pincer complex has been synthesized by metalation and transmetalation procedures. The deprotonation of the less acidic C5 protons of the imidazole-based proligand was achieved using $Zr(NMe_2)_4$. The Pt pincer complex has distorted square-planar configurations as expected for d^8 four-coordinated transition-metal compounds. The cationic Pt adduct binds strongly to the N_2 in the gas phase. The mass spectra revealed that the cationic dinitrogen Pt(II) pincer complex is a potential synthetic compound to be looked at in the future. The CID-MS studies indicated more energy input was required to disrupt the N_2 complex than the MeCN complex within the gas-phase environment of the ion trap and within the time scale of the CID-MS experiment. DFT calculations revealed that N_2 weakly binds to the cationic CCC-NHC Pt(II) pincer complexes compared to MeCN. The DFT calculations predicted that the dissociation of the N_2 from the Pt complex was kinetically favored over the MeCN complex based on transition states located on the potential energy surface. Thermodynamically, the MeCN complex was predicted to be more stable than the N_2 complex. The computational results reconciled the MS experiments suggesting a higher kinetic barrier for N_2 dissociation due to what is effectively tumbling of the N_2 in the coordination sphere of the Pt. This path is not available in the MeCN due to symmetry constraints. The CCC-aNHC Pt(II) complex is among the observed complexes of platinum that bind to dinitrogen molecules in the gas phase. The reactivity and isolation of the Pt N_2 complexes are still ongoing investigations in our lab.

EXPERIMENTAL DETAILS

General Procedures. All starting materials were purchased from Sigma-Aldrich, Fisher Scientific, or Strem. The reagents were used as received unless otherwise mentioned. All solvents were dried and degassed by passing through a basic alumina column under N_2 protection. All reactions involving organometallic reagents were carried out under a N_2 atmosphere using a standard glovebox. NMR spectra were collected using a Bruker Advance 500 spectrometer and were referenced to the residual solvent peak (δ in ppm, J in Hz). Electrospray ionization mass spectra were collected using a Waters Micromass ZQ mass spectrometer.

Synthesis of 1,3-(2-phenylimidazole) Benzene (7). Compound 7 was prepared by combining 1,3-bromobenzene (5.0 mL, 41.33 mmol), 2-phenylimidazole (17.88 g, 123.99 mmol), K_2CO_3 (17.14 g, 123.99 mmol), CuO (3.0 g, 37.7 mmol), and DMSO (60 mL). The mixture was heated at 160 °C for 96 h. The reaction was cooled to room temperature, and 250 mL of CH_2Cl_2 was added and then passed through silica gel. The silica gel was eluted with 800 mL of CH_2Cl_2/IPA (10:1). The solvent was evaporated at reduced pressure to obtain a dark brown solid. The solid was washed with 150 mL acetone to give a white solid (7.07 g, 47%). ^{1}H NMR (500 MHz, $CDCl_3$): δ 7.11 (pseudo-t, J = 5 Hz, 1H), 7.03 (s, 2 H), 7.47 (d, J = 10 Hz, 2H), 7.23 (s, 2H), 7.31 (m, 5H), 7.40−7.44 (m, 5H). ^{13}C{^{1}H} NMR (125 MHz, $CDCl_3$): δ 144.5, 137.2, 128.2, 127.7, 124.5, 126.0 123.1, 120.9, 120.1. ESI-MS calcd for $C_{24}H_{19}N_4$ $[M + H]^+$ m/z = 363.1610, found m/z = 363.1658.

Synthesis of 1,3-Bis(N-butyl-2-phenylimidazolium)benzene Diiodide (8). Compound 8 was prepared by combining 1,3-(2-phenylimidazole) benzene (1.50 g, 4.14 mmol), 1-butyl iodide (8.05 g, 41.4 mmol) in 40 mL of acetonitrile, heated at 120 °C for 48 h. The resulting brown solution was cooled to room temperature, and the solvent was removed under reduced pressure, yielding yellowish solids. The solids were dissolved in acetone to recrystallize in about 3 min to give white crystals (2.92 g, 96%). ^{1}H NMR (500 MHz, CD_2Cl_2): δ 8.44 (s, 1H), 8.0 (s, 2H), 7.81 (s, 2H), 7.77 (d, J = 5 Hz, 4H), 7.57 (t, J = 10 Hz, 2H), 7.53 (d, J = 10 Hz, 2H), 7.47 (t, J = 10 Hz, 4H), 7.21 (t, J = 10 Hz, 1H), 4.13 (t, J = 5 Hz, 4H), 1.87 (m, 4H), 1.32 (m, 4H), 0.84 (t, J = 5 Hz, 6H). ^{13}C{^{1}H} NMR (125 MHz, CD_2Cl_2): δ 158.4, 149.4, 146.2, 144.8, 143.2, 142.8, 142.4, 139.2, 137.6, 136.7, 134.9, 62.2, 45.0, 32.7, 27.1 ESI-MS calcd for $C_{32}H_{36}IN_4$ $[M - I]^+$ m/z = 603.1985, ound m/z = 603.2061. ESI-MS calcd for $C_{32}H_{36}N_4$ $[M - 2I]^{2+}$ m/z = 238.1465, found m/z = 238.1495.

Synthesis 2-(1,3-Bis(N-butyl-2-phenylimidazolium)-phenylene)(iodo)platinum(II) (9). The salt 1,3-bis(N-butyl-2-phenylimidazolium)benzene diiodide (0.300 g, 0.410 mmol), $Zr(NMe_2)_4$ (0.275 g, 1.03 mmol), and 10 mL of CH_2Cl_2 were combined, providing a clear colorless solution. After stirring at room temperature for 17 h, the solution changed to pale yellow in color. After 17 h reaction time, $[PtCl_2(COD)]$ (0.230 g, 0.615 mmol) was added to the pale-yellow solution, and stirring continued at room temperature for another 20 min. The reaction mixture was transferred to a round-bottom flask that contained 1.5 mL of distilled water, and the precipitate was removed by filtering through Celite. The clear yellow solution was concentrated under reduced pressure, yielding yellow solids. The solids were triturated with ether followed by 9:1 acetone/water (3 × 2 mL) to remove any dimethylammonium salt. It was then put back on the rotavap at a temperature of 60 °C, yielding yellow powdery solids (0.264 g, 84%). X-ray quality crystals were grown by slow diffusion of diethyl ether vapor into a CH_2Cl_2 solution. ^{1}H NMR ($CDCl_3$, 500 MHz): δ 7.68 (t, 2H), 7.63 (t, J = 5 Hz, 4H), 7.45 (d, J = 10 Hz, 4H), 7.22 (s, 2H, $^3J_{Pt-H}$ = 5 Hz, im-H), 6.39 (t, J = 10 Hz, 1H), 5.85 (d, J = 10 Hz, 2H, $^4J_{Pt-H}$ = 25 Hz, m-Ph), 3.75 (t, J = 10 Hz, 4H), 1.74 (m, 4H), 1.26 (m, 4H), 0.86 (t, J = 10 Hz, 6H). ^{13}C{^{1}H} NMR ($CDCl_3$, 125 MHz): 157.6 ($^1J_{Pt-C}$ = 6715 Hz), 146.4 ($^1J_{Pt-C}$ = 60 Hz), 140.3, 140.0, 132.1, 130.7, 130.1, 125.7, 125.2, 121.2, 112.2, 47.3, 32.6, 20.1, 13.8. ESI-MS calcd for $C_{32}H_{33}N_4Pt$ [M

https://doi.org/10.1021/acs.organomet.3c00411
Organometallics XXXX, XXX, XXX−XXX

− I]$^+$ m/z = 668.2353, found m/z = 668.2355. ESI-MS calcd for $C_{32}H_{33}N_6Pt$ [M + N_2]$^+$ m/z = 696.2414, found m/z = 696.2375. ESI-MS calcd for $C_{34}H_{36}N_5Pt$ [M + MeCN]$^+$ m/z = 709.2618, found m/z = 709.2577. Anal. Calcd for $C_{32}H_{33}N_4IPt$: C, 48.31; H, 4.18; N, 7.04; found: C, 48.66; H, 4.17; N, 6.89.

Collision-Induced Dissociation (CID). CID-MS was conducted on an LTQ Velos spectrometer using an ESI source in the positive mode. The sample was introduced via direct infusion at a flow rate of 3.0 μL/min. The spray voltage and capillary temperature were maintained at 4.0 kV and 275 °C, respectively. Nitrogen was utilized as the sheath gas, while helium was the collision gas. The CID experiment was carried out between NCE 0 and 30 in steps of 1 NCE, and the curve was generated by plotting the percentage of remaining precursor ion (precursor ion intensity/summed precursor and product ion intensities multiplied by 100) as a function of collision energy.

X-ray Crystallography. A yellow prism single crystal of $C_{64}H_{65}I_2N_8Pt_2$, approximate dimensions 0.105 × 0.155 × 0.469) mm^3, was selected for the X-ray crystallographic analysis and mounted on a cryoloop using an oil cryoprotectant. The X-ray intensity data were measured at a low temperature (T = 100 K), using a three-circle geometry goniometer with a fixed Chie angle at = 54.74° Bruker AXS D8 Venture, equipped with a Photon 100 CMOS active pixel sensor detector. Monochromatized Cu X-ray radiation (λ = 1.54178 Å) was selected for the measurement. All frames were integrated with the aid of the Bruker SAINT software using a narrow-frame algorithm. The integration of the data using a triclinic unit cell yielded a total of 14 776 reflections to a maximum θ angle of 66.60° (0.84 Å resolution), of which 9511 were independent (average redundancy 1.554, completeness = 96.5%, R_{int} = 4.63%, R_{sig} = 5.58%) and 8718 (91.66%) were greater than 2σ (F^2). The final cell constants of a = 13.3360(15) Å, b = 13.8619(15) Å, c = 17.1291(19) Å, α = 79.370(4) °, β = 72.301(4) °, γ = 68.098(3) °, and volume = 2789.9(5) Å^3 are based upon the refinement of the 3797 XYZ centroids of reflections above 20σ (I). Data were corrected for absorption effects using the Multi-Scan method (TWINABS). The calculated minimum and maximum transmission coefficients (based on crystal size) are 0.0420 and 0.2490. The structure was solved in a monoclinic unit cell. Centrosymmetric space group: $P12(1)/n1$, with Z = 4 for the formula unit, $C_{64}H_{65}I_2N_8Pt_2$. Using the Bruker SHELXT Software Package, refinement of the structure was carried out by least-squares procedures on weighted F^2 values using the SHELXTL-2018/3 program included in the APEX4 v2021, 10.0, AXS Bruker program. The asymmetric unit was built on two independent molecules respectively labeled A and B. A nonmerohedral twinning was detected using the program Cell_now integrated into the APEX4 v2021, 10.0, AXS Bruker program. Hydrogen atoms were localized on different Fourier maps but then were introduced in the refinement as fixed contributors in idealized geometry with isotropic thermal parameters fixed at 20% higher than those carbon atoms to which they were connected. The final anisotropic full-matrix least-squares refinement on F^2 with 684 variables converged at R1 = 4.84% for the observed data and wR2 = 15.16% for all data. Restraints were added on an ADP's parameters. Some unexplained electronic densities in the vicinity of the Pt atoms remained. The goodness-of-fit (GOF) was 1.049. The largest peak in the final difference electron density synthesis was 2.938 e-/Å3 and the largest hole was −1.619 e-/Å3 with an RMS deviation of 0.302 e-/Å3. Based on the final model, the calculated density was 1.893 g/cm^3 and F (000) was 1534 e-. Graphics were created using the Mercury V.4.2.0 software (https://www.ccdc.cam.ac.uk/) and POV-Ray v 3.7 (The Persistence of Vision Raytracer, high quality, Free Software tool).

Computational Details. The reported structures are fully optimized in the Gaussian 16 software.[55] The PBE1PBE density functional[55,56] with the D3 version of the Grimme dispersion correction with Becke-Johnson damping was used at the BS1 basis set level theory (where BS1 is the electron core potential and the modified LANL2DZ basis set[57] was used for Pt and the 6-31G(d′) basis sets for the remaining atoms). To account for solvation effects, single-point calculations with the SMD implicit model[58] using acetonitrile parameters were performed on the optimized gas-phase geometry. The results from the DFT calculations were verified with single-point calculations using the DLPNO−CCSD(T) method[59] at the BS2 level of theory in the ORCA (version 5) package.[60] For BS2, auxiliary quadruple-ζ basis set def2-QZVPP[61] was used.

■ ASSOCIATED CONTENT

Supporting Information

The Supporting Information is available free of charge at https://pubs.acs.org/doi/10.1021/acs.organomet.3c00411.

^{1}H and ^{13}C NMR spectra, mass spectrometry, CID, X-ray, and computational data for new compounds (PDF)

Cartesian coordinates for the computed structures (XYZ)

Accession Codes

CCDC 2201811 contains the supplementary crystallographic data for this paper. These data can be obtained free of charge via www.ccdc.cam.ac.uk/data_request/cif, or by emailing data_request@ccdc.cam.ac.uk, or by contacting The Cambridge Crystallographic Data Centre, 12 Union Road, Cambridge CB2 1EZ, UK; fax: +44 1223 336033.

■ AUTHOR INFORMATION

Corresponding Authors

Amanda L. Patrick − *Department of Chemistry, Center for Computational Sciences, Mississippi State University, Mississippi State, Mississippi 39762, United States;* orcid.org/0000-0003-4525-0970; Email: apatrick@chemistry.msstate.edu

Charles Edwin Webster − *Department of Chemistry, Center for Computational Sciences, Mississippi State University, Mississippi State, Mississippi 39762, United States;* orcid.org/0000-0002-6917-2957; Email: ewebster@chemistry.msstate.edu

T. Keith Hollis − *Department of Chemistry, Center for Computational Sciences, Mississippi State University, Mississippi State, Mississippi 39762, United States;* orcid.org/0000-0002-5470-9811; Email: khollis@chemistry.msstate.edu

Authors

Evans Fosu − *Department of Chemistry, Center for Computational Sciences, Mississippi State University, Mississippi State, Mississippi 39762, United States*

Nghia Le − *Department of Chemistry, Center for Computational Sciences, Mississippi State University, Mississippi State, Mississippi 39762, United States*

Taofiq Abdulraheem − *Department of Chemistry, Center for Computational Sciences, Mississippi State University, Mississippi State, Mississippi 39762, United States*

Bruno Donnadieu − *Department of Chemistry, Center for Computational Sciences, Mississippi State University, Mississippi State, Mississippi 39762, United States*

Complete contact information is available at: https://pubs.acs.org/10.1021/acs.organomet.3c00411

Notes

The authors declare no competing financial interest.

■ ACKNOWLEDGMENTS

We gratefully acknowledge the National Science Foundation for grants NSF OIA 1539035 and NSF PFI-TT 1827686 and

the Department of Chemistry, Mississippi State University for financial support. We thank Wallinger Jayna for assistance with plotting the CID data.

REFERENCES

(1) Nørskov, J.; Chen, J.; Miranda, R.; Fitzsimmons, T.; Stack, R. *Sustainable Ammonia Synthesis—Exploring the Scientific Challenges Associated with Discovering Alternative, Sustainable Processes for Ammonia Production*; US DOE Office of Science, 2016.

(2) (a) Maxwell, G. R. Uses of ammonia. *Synthetic Nitrogen Products: A Practical Guide to the Products and Processes*; Springer, 2004; pp 199−203. (b) Timmer, B.; Olthuis, W.; van den Berg, A. Ammonia sensors and their applications—a review. *Sensors Actuators B: Chem.* **2005**, *107* (2), 666−677.

(3) Afanasyev, O. I.; Kuchuk, E.; Usanov, D. L.; Chusov, D. Reductive amination in the synthesis of pharmaceuticals. *Chem. Rev.* **2019**, *119* (23), 11857−11911.

(4) Lancaster, K. M.; Roemelt, M.; Ettenhuber, P.; Hu, Y.; Ribbe, M. W.; Neese, F.; Bergmann, U.; DeBeer, S. X-ray emission spectroscopy evidences a central carbon in the nitrogenase iron-molybdenum cofactor. *Science* **2011**, *334* (6058), 974−977.

(5) (a) Kim, J.; Rees, D. Structural models for the metal centers in the nitrogenase molybdenum-iron protein. *Science* **1992**, *257* (5077), 1677−1682. (b) Smith, B. E. Nitrogenase reveals its inner secrets. *Science* **2002**, *297* (5587), 1654−1655.

(6) Schlögl, R. Catalytic Synthesis of Ammonia—A "Never-Ending Story"? *Angew. Chem., Int. Ed.* **2003**, *42* (18), 2004−2008.

(7) Tanabe, Y.; Nishibayashi, Y. Comprehensive insights into synthetic nitrogen fixation assisted by molecular catalysts under ambient or mild conditions. *Chem. Soc. Rev.* **2021**, *50* (8), 5201−5242.

(8) (a) Sheu, E. J.; Mokheimer, E. M.; Ghoniem, A. F. A review of solar methane reforming systems. *Int. J. Hydrogen Energy* **2015**, *40* (38), 12929−12955. (b) Taherian, Z.; Khataee, A.; Han, N.; Orooji, Y. Hydrogen production through methane reforming processes using promoted-Ni/mesoporous silica: A review. *J. Ind. Eng. Chem.* **2022**, *107*, 20−30.

(9) (a) Ghavam, S.; Vahdati, M.; Wilson, I.; Styring, P. Sustainable ammonia production processes. *Front. Energy Res.* **2021**, *9*, No. 580808.

(10) Haruyama, T.; Namise, T.; Shimoshimizu, N.; Uemura, S.; Takatsuji, Y.; Hino, M.; Yamasaki, R.; Kamachi, T.; Kohno, M. Non-catalyzed one-step synthesis of ammonia from atmospheric air and water. *Green Chem.* **2016**, *18* (16), 4536−4541.

(11) Hidai, M.; Mizobe, Y. Recent advances in the chemistry of dinitrogen complexes. *Chem. Rev.* **1995**, *95* (4), 1115−1133.

(12) (a) Allen, A.; Harris, R.; Loescher, B.; Stevens, J.; Whiteley, R. Dinitrogen complexes of the transition metals. *Chem. Rev.* **1973**, *73* (1), 11−20. (b) Gambarotta, S. Dinitrogen fixation and activation after 30 years: a puzzle still unsolved. *J. Organomet. Chem.* **1995**, *500* (1−2), 117−126.

(13) Allen, A.; Senoff, C. Nitrogenopentammineruthenium (II) complexes. *Chemical Communications (London)* **1965**, *24*, 621−622.

(14) (a) Ohki, Y.; Fryzuk, M. D. Dinitrogen activation by group 4 metal complexes. *Angew. Chem., Int. Ed.* **2007**, *46* (18), 3180−3183. (b) MacKay, B. A.; Fryzuk, M. D. Dinitrogen coordination chemistry: on the biomimetic borderlands. *Chem. Rev.* **2004**, *104* (2), 385−402.

(15) Stucke, N.; Weyrich, T.; Pfeil, M.; Grund, K.; Kindjajev, A.; Tuczek, F. Synthetic Nitrogen Fixation with Mononuclear Molybdenum (0) Phosphine Complexes: Occupying the trans-Position of Coordinated N 2. *Nitrogen Fixation* **2017**, *60*, 113−152.

(16) (a) Fryzuk, M. D. Side-on end-on bound dinitrogen: An activated bonding mode that facilitates functionalizing molecular nitrogen. *Acc. Chem. Res.* **2009**, *42* (1), 127−133. (b) Cummins, D. C.; Yap, G. P.; Theopold, K. H. Scorpionates of the "Tetrahedral Enforcer" Variety as Ancillary Ligands for Dinitrogen Complexes of First Row Transition Metals (Cr−Co). *Eur. J. Inorg. Chem.* **2016**, *2016* (15−16), 2349−2356.

(17) (a) Grohmann, A. Tetrapodal pentadentate ligands: Single site reactivity and bond activation in iron (II) complexes. *Dalton Trans.* **2010**, *39* (6), 1432−1440. (b) Grohmann, A. Tetrapodal pentadentate nitrogen ligands: Aspects of complex structure and reactivity. *Adv. Inorg. Chem.* **2004**, *56*, 179−210.

(18) (a) Hazari, N. Homogeneous iron complexes for the conversion of dinitrogen into ammonia and hydrazine. *Chem. Soc. Rev.* **2010**, *39* (11), 4044−4056. (b) Kim, S.; Loose, F.; Chirik, P. J. Beyond ammonia: nitrogen−element bond forming reactions with coordinated dinitrogen. *Chem. Rev.* **2020**, *120* (12), 5637−5681.

(19) (a) Emerson-King, J.; Pan, S.; Gyton, M. R.; Tonner-Zech, R.; Chaplin, A. B. Synthesis of a rhodium (iii) dinitrogen complex using a calix [4] arene-based diphosphine ligand. *Chem. Commun.* **2023**, *59* (15), 2150−2152. (b) Junge, J.; Engesser, T. A.; Krahmer, J.; Näther, C.; Tuczek, F. Rhodium (III) and Ruthenium (II) Complexes with a Pentadentate Tetrapodal Phosphine Ligand. *Z. Anorg. Allg. Chem.* **2021**, *647* (8), 822−831. (c) Tanabe, Y.; Nishibayashi, Y. Recent advances in catalytic nitrogen fixation using transition metal−dinitrogen complexes under mild reaction conditions. *Coord. Chem. Rev.* **2022**, *472*, 214783. (d) Bora, D.; Gayen, F. R.; Saha, B. Ammonia from dinitrogen at ambient conditions by organometallic catalysts. *RSC Adv.* **2022**, *12* (52), 33567−33583. (e) Nishibayashi, Y. Recent progress in transition-metal-catalyzed reduction of molecular dinitrogen under ambient reaction conditions. *Inorg. Chem.* **2015**, *54* (19), 9234−9247.

(20) (a) Holland, P. L. Metal−dioxygen and metal−dinitrogen complexes: where are the electrons? *Dalton Trans.* **2010**, *39* (23), 5415−5425. (b) Holze, P.; Horn, B.; Limberg, C.; Matlachowski, C.; Mebs, S. The Activation of Sulfur Hexafluoride at Highly Reduced Low-Coordinate Nickel Dinitrogen Complexes. *Angew. Chem., Int. Ed.* **2014**, *53* (10), 2750−2753.

(21) (a) Walter, M. Recent advances in transition metal-catalyzed dinitrogen activation. *Adv. Organomet. Chem.* **2016**, *65*, 261−377. (b) Mindiola, D. J. Nacnac... Are You Still There? The Evolution of β-Diketiminate Complexes of Nickel. *Angew. Chem., Int. Ed.* **2009**, *48* (34), 6198−6200.

(22) Holze, P.; Braun-Cula, B.; Mebs, S.; Limberg, C. Stabilization of β-Diketiminato Nickel (I) with Alkaline Metal Halide Entities for Small Molecule Activation. *Z. Anorg. Allg. Chem.* **2018**, *644* (17), 973−981.

(23) Ozin, G.; Klotzbücher, W. Binary mixed dioxygen dinitrogen complexes of nickel, palladium, and platinum,(O2) M (N2) n (where M= nickel, palladium, or platinum; n= 1 or 2). *J. Am. Chem. Soc.* **1975**, *97* (14), 3965−3974.

(24) (a) Black, M.; Mais, R.; Owston, P. The crystal and molecular structure of Zeise's salt, KPtCl3. C2H4. H2O. *Acta Crystallographica Section B: Structural Crystallography and Crystal Chemistry* **1969**, *25* (9), 1753−1759. (b) Hiraishi, J. The vibrational spectra of several platinum-ethylene complexes: K [PtCl3 (C2H4)]·H2O (Zeise's salt), K [PtCl3 (C2D4)]·H2O and [PtCl2(C2H4)]2. *Spectrochim. Acta, Pt. A: Mol. Spectrosc.* **1969**, *25* (4), 749−760. (c) Jarvis, J.; Kilbourn, B.; Owston, P. A re-determination of the crystal and molecular structure of Zeise's salt, KPtCl3. C2H4. H2O. *Acta Crystallographica Section B: Structural Crystallography and Crystal Chemistry* **1971**, *27* (2), 366−372. (d) Luinstra, G. A.; Wang, L.; Stahl, S. S.; Labinger, J. A.; Bercaw, J. E. Oxidation of Zeise's salt by [PtCl6] 2-: a mechanistic model for hydrocarbon oxidation. *Organometallics* **1994**, *13* (3), 755−756.

(25) (a) Thomas, G. T.; Donnecke, S.; Paci, I.; McIndoe, J. S. Trichloro(Dinitrogen)Platinate (II). *Chemistry−A European Journal* **2020**, *26* (54), 12359−12362. (b) Wentrup, C. Zeise, Liebig, Jensen, Hückel, Dewar, and the Olefin π-Complex Bonds. *Angew. Chem., Int. Ed.* **2020**, *59* (22), 8332−8342.

(26) Feifan, X.; Pieter, C.; Jan, V. B. Electrospray ionization mass spectrometry for the hydrolysis complexes of cisplatin: implications for the hydrolysis process of platinum complexes. *J. Mass Spectrom.* **2017**, *52* (7), 434−441.

https://doi.org/10.1021/acs.organomet.3c00411
Organometallics XXXX, XXX, XXX−XXX

(27) Greis, K.; Yang, Y.; Canty, A. J.; O'Hair, R. A. Gas-phase synthesis and reactivity of ligated group 10 ions in the formal+ 1 oxidation state. *J. Am. Soc. Mass. Spectrom.* **2019**, *30* (10), 1867−1880.
(28) Chianese, A. R.; Kovacevic, A.; Zeglis, B. M.; Faller, J.; Crabtree, R. H. Abnormal C5-bound N-heterocyclic carbenes: Extremely strong electron donor ligands and their iridium (I) and iridium (III) complexes. *Organometallics* **2004**, *23* (10), 2461−2468.
(29) (a) Hussaini, S. Y.; Haque, R. A.; Razali, M. R. Recent progress in silver (I)-, gold (I)/(III)-and palladium (II)-N-heterocyclic carbene complexes: A review towards biological perspectives. *J. Organomet. Chem.* **2019**, *882*, 96−111. (b) Lin, J. C.; Huang, R. T.; Lee, C. S.; Bhattacharyya, A.; Hwang, W. S.; Lin, I. J. Coinage metal−N-heterocyclic carbene complexes. *Chem. Rev.* **2009**, *109* (8), 3561−3598. (c) Zhao, S.; Yang, Z.; Jiang, G.; Huang, S.; Bian, M.; Lu, Y.; Liu, W. An overview of anticancer platinum N-heterocyclic carbene complexes. *Coord. Chem. Rev.* **2021**, *449*, 214217.
(30) Herrmann, W. A. N-heterocyclic carbenes: a new concept in organometallic catalysis. *Angew. Chem., Int. Ed.* **2002**, *41* (8), 1290−1309.
(31) (a) Shen, H.; Tian, G.; Xu, Z.; Wang, L.; Wu, Q.; Zhang, Y.; Teo, B. K.; Zheng, N. N-heterocyclic carbene coordinated metal nanoparticles and nanoclusters. *Coord. Chem. Rev.* **2022**, *458*, 214425. (b) Ibrahim, H.; Bala, M. D.; Friedrich, H. B. Poly-functional imino-N-heterocyclic carbene ligands: Synthesis, complexation, and catalytic applications. *Coord. Chem. Rev.* **2022**, *469*, 214652.
(32) Nasr, A.; Winkler, A.; Tamm, M. Anionic N-heterocyclic carbenes: Synthesis, coordination chemistry and applications in homogeneous catalysis. *Coord. Chem. Rev.* **2016**, *316*, 68−124.
(33) Ma, X.; Guillet, S. G.; Liu, Y.; Cazin, C. S.; Nolan, S. P. Simple synthesis of [Ru (CO 3)(NHC)(p-cymene)] complexes and their use in transfer hydrogenation catalysis. *Dalton Trans.* **2021**, *50* (37), 13012−13019.
(34) (a) Gruendemann, S.; Kovacevic, A.; Albrecht, M.; Faller, J. W.; Crabtree, R. H. Abnormal ligand binding and reversible ring hydrogenation in the reaction of imidazolium salts with IrH5 (PPh3) 2. *J. Am. Chem. Soc.* **2002**, *124* (35), 10473−10481. (b) Aldeco-Perez, E.; Rosenthal, A. J.; Donnadieu, B.; Parameswaran, P.; Frenking, G.; Bertrand, G. Isolation of a c5-deprotonated imidazolium, a crystalline abnormal n-heterocyclic carbene. *Science* **2009**, *326* (5952), 556−559.
(35) (a) Danopoulos, A. A.; Massard, A.; Frison, G.; Braunstein, P. Iron and Cobalt Metallotropism in Remote-Substituted NHC Ligands: Metalation to Abnormal NHC Complexes or NHC Ring Opening. *Angew. Chem.* **2018**, *130* (44), 14758−14762. (b) Manzano, R.; Rominger, F.; Hashmi, A. S. K. Saturated abnormal NHC−Gold (I) complexes: synthesis and catalytic activity. *Organometallics* **2013**, *32* (7), 2199−2203. (c) Schnee, G.; Nieto Faza, O.; Specklin, D.; Jacques, B.; Karmazin, L.; Welter, R.; Silva López, C.; Dagorne, S. Normal-to-Abnormal NHC Rearrangement of AlIII, GaIII, and InIII Trialkyl Complexes: Scope, Mechanism, Reactivity Studies, and H2 Activation. *Chemistry−A European Journal* **2015**, *21* (49), 17959−17972. (d) Zuo, W.; Braunstein, P. N-heterocyclic dicarbene iridium (III) pincer complexes featuring mixed NHC/abnormal NHC ligands and their applications in the transfer dehydrogenation of cyclooctane. *Organometallics* **2012**, *31* (7), 2606−2615. (e) Hashmi, A. S. K.; Riedel, D.; Rudolph, M.; Rominger, F.; Oeser, T. Regioselective formation of saturated abnormal NHC−gold (I) complexes by [3+ 2] cycloaddition of azomethine ylides and isonitrile gold (I) complexes. *Chemistry−A European Journal* **2012**, *18* (13), 3827−3830. (f) Ghadwal, R. S.; Lamm, J.-H.; Rottschäfer, D.; Schürmann, C. J.; Demeshko, S. Facile routes to abnormal-NHC-cobalt (II) complexes. *Dalton Trans.* **2017**, *46* (24), 7664−7667. (g) Grineva, A. A.; Filippov, O. A.; Canac, Y.; Sortais, J.-B.; Nefedov, S. E.; Lugan, N.; César, V.; Valyaev, D. A. Experimental and theoretical insights into the electronic properties of anionic N-heterocyclic dicarbenes through the rational synthesis of their transition metal complexes. *Inorg. Chem.* **2021**, *60* (6), 4015−4025. (h) Das, A.; Chakraborty, S.; Mandal, S. K. Abnormal N-heterocyclic Carbene Based Ni (II) π-allyl Complex towards Molecular Oxygen Activation. *Chemistry−An Asian Journal* **2021**, *16* (16), 2257−2260. (i) Krüger, A.; Häller, L. J. L.; Müller-Bunz, H.; Serada, O.; Neels, A.; Macgregor, S. A.; Albrecht, M. Smooth C (alkyl)−H bond activation in rhodium complexes comprising abnormal carbene ligands. *Dalton Trans.* **2011**, *40* (38), 9911−9920. (j) Krüger, A.; Neels, A.; Albrecht, M. Rhodium-mediated activation of an alkane-type C−H bond. *Chem. Commun.* **2010**, *46* (2), 315−317.
(36) (a) Crabtree, R. H. Abnormal, mesoionic and remote N-heterocyclic carbene complexes. *Coord. Chem. Rev.* **2013**, *257* (3−4), 755−766. (b) Perrin, L.; Clot, E.; Eisenstein, O.; Loch, J.; Crabtree, R. H. Computed ligand electronic parameters from quantum chemistry and their relation to Tolman parameters, lever parameters, and Hammett constants. *Inorg. Chem.* **2001**, *40* (23), 5806−5811.
(37) (a) Tan, K. V.; Li, Z.; Karmis, R. E.; Barnard, P. J. Selective Synthesis of Ni (II) and Pd (II) Complexes with either 'Normal'or 'Abnormal'N-Heterocyclic Carbene Coordination Modes. *Chemistry-Select* **2018**, *3* (10), 2830−2836. (b) Lee, J.-Y.; Hsieh, M.-J.; Ho, T.-E.; Wu, B.-H.; Lee, H. M. Nickel (ii) complexes containing tridentate ONC i ligands (i= abnormal N-heterocyclic carbene donors) and their catalytic application in Suzuki−Miyaura coupling reaction. *Dalton Trans.* **2022**, *51* (17), 6663−6672.
(38) (a) Van Vuuren, E.; Malan, F. P.; Landman, M. Multidentate NHC complexes of group IX metals featuring carbon-based tethers: Synthesis and applications. *Coord. Chem. Rev.* **2021**, *430*, 213731. (b) Baltrun, M.; Watt, F. A.; Schoch, R.; Wölper, C.; Neuba, A. G.; Hohloch, S. A new bis-phenolate mesoionic carbene ligand for early transition metal chemistry. *Dalton Trans.* **2019**, *48* (39), 14611−14625.
(39) Romain, C.; Bellemin-Laponnaz, S.; Dagorne, S. Recent progress on NHC-stabilized early transition metal (group 3−7) complexes: Synthesis and applications. *Coord. Chem. Rev.* **2020**, *422*, 213411.
(40) Gründemann, S.; Albrecht, M.; Loch, J. A.; Faller, J. W.; Crabtree, R. H. Tridentate carbene CCC and CNC pincer palladium (II) complexes: structure, fluxionality, and catalytic activity. *Organometallics* **2001**, *20* (25), 5485−5488.
(41) Normand, A. T. N-heterocylic and mesoionic carbene complexes of the group 4 metals. *Reference Module in Chemistry, Molecular Sciences and Chemical Engineering*; Elsevier, 2020.
(42) Poyatos, M.; Mata, J. A.; Falomir, E.; Crabtree, R. H.; Peris, E. New ruthenium (II) CNC-pincer bis (carbene) complexes: Synthesis and catalytic activity. *Organometallics* **2003**, *22* (5), 1110−1114.
(43) (a) Danopoulos, A. A.; Wright, J. A.; Motherwell, W. B.; Ellwood, S. N-Heterocyclic "Pincer" Dicarbene Complexes of Cobalt(I), Cobalt(II), and Cobalt(III). *Organometallics* **2004**, *23* (21), 4807−4810. (b) Danopoulos, A. A.; Tsoureas, N.; Wright, J. A.; Light, M. E. N-Heterocyclic Pincer Dicarbene Complexes of Iron(II): C-2 and C-5 Metalated Carbenes on the Same Metal Center. *Organometallics* **2004**, *23* (2), 166−168. (c) McGuinness, D. S.; Gibson, V. C.; Wass, D. F.; Steed, J. W. Bis(carbene)pyridine Complexes of Cr(III): Exceptionally Active Catalysts for the Oligomerization of Ethylene. *J. Am. Chem. Soc.* **2003**, *125* (42), 12716−12717. (d) Pugh, D.; Wells, N. J.; Evans, D. J.; Danopoulos, A. A. Reactions of 'pincer'pyridine dicarbene complexes of Fe (0) with silanes. *Dalton Trans.* **2009**, *35*, 7189−7195.
(44) (a) Rubio, R. J.; Andavan, G. T. S.; Bauer, E. B.; Hollis, T. K.; Cho, J.; Tham, F. S.; Donnadieu, B. Toward a general method for CCC N-heterocyclic carbene pincer synthesis: Metallation and transmetallation strategies for concurrent activation of three C−H bonds. *J. Organomet. Chem.* **2005**, *690* (23), 5353−5364. (b) Helgert, T. R.; Hollis, T. K.; Oliver, A. G.; Valle, H. U.; Wu, Y.; Webster, C. E. Synthesis, characterization, and X-ray molecular structure of tantalum CCC-N-heterocyclic carbene (CCC-NHC) pincer complexes with imidazole-and triazole-based ligands. *Organometallics* **2014**, *33* (4), 952−958. (c) Matson, E. M.; Espinosa Martinez, G.; Ibrahim, A. D.; Jackson, B. J.; Bertke, J. A.; Fout, A. R. Nickel(II) Pincer Carbene Complexes: Oxidative Addition of an Aryl C−H Bond to Form a Ni(II) Hydride. *Organometallics* **2015**, *34* (2), 399−407. (d) Taakili,

https://doi.org/10.1021/acs.organomet.3c00411
Organometallics XXXX, XXX, XXX−XXX

R.; Canac, Y. NHC core pincer ligands exhibiting two anionic coordinating extremities. *Molecules* **2020**, *25* (9), 2231.
(45) (a) Vivancos, A. n.; Segarra, C.; Albrecht, M. Mesoionic and related less heteroatom-stabilized N-heterocyclic carbene complexes: synthesis, catalysis, and other applications. *Chem. Rev.* **2018**, *118* (19), 9493−9586. (b) Song, G.; Zhang, Y.; Li, X. Rhodium and iridium complexes of abnormal N-heterocyclic carbenes derived from imidazo [1, 2-a] pyridine. *Organometallics* **2008**, *27* (8), 1936−1943. (c) Poulain, A.; Canseco-Gonzalez, D.; Hynes-Roche, R.; Müller-Bunz, H.; Schuster, O.; Stoeckli-Evans, H.; Neels, A.; Albrecht, M. Synthesis and tunability of abnormal 1, 2, 3-triazolylidene palladium and rhodium complexes. *Organometallics* **2011**, *30* (5), 1021−1029. (d) Maity, R.; Sarkar, B. Chemistry of compounds based on 1, 2, 3-triazolylidene-type mesoionic carbenes. *JACS Au* **2022**, *2* (1), 22−57.
(46) (a) Yan, X.; Wang, H.; Guo, S. Employing Aryl-Linked Bis-mesoionic Carbenes as a Pincer-Type Platform to Access Ambient-Stable Palladium (IV) Complexes. *Angew. Chem., Int. Ed.* **2019**, *58* (47), 16907−16911. (b) Rendón-Nava, D.; Angeles-Beltrán, D.; Rheingold, A. L.; Mendoza-Espinosa, D. Palladium (II) Complexes of a Neutral CCC-Tris (N-heterocyclic carbene) Pincer Ligand: Synthesis and Catalytic Applications. *Organometallics* **2021**, *40* (13), 2166−2177. (c) Mondal, T.; De, S.; Dutta, S.; Koley, D. Mechanistic exploration of the transmetalation and reductive elimination events involving PdIV−abnormal NHC complexes in Suzuki−Miyaura coupling reactions: a DFT study. *Chemistry−A European Journal* **2018**, *24* (23), 6155−6168.
(47) (a) Clark, W. D.; Cho, J.; Valle, H. U.; Hollis, T. K.; Valente, E. J. Metal and halogen dependence of the rate effect in hydroamination/cyclization of unactivated aminoalkenes: Synthesis, characterization, and catalytic rates of CCC-NHC hafnium and zirconium pincer complexes. *J. Organomet. Chem.* **2014**, *751*, 534−540. (b) Cho, J.; Hollis, T. K.; Helgert, T. R.; Valente, E. J. An improved method for the synthesis of zirconium (CCC-N-heterocyclic carbene) pincer complexes and applications in hydroamination. *Chem. Commun.* **2008**, *40*, 5001−5003. (c) Reilly, S. W.; Webster, C. E.; Hollis, T. K.; Valle, H. U. Transmetallation from CCC-NHC pincer Zr complexes in the synthesis of air-stable CCC-NHC pincer Co (III) complexes and initial hydroboration trials. *Dalton Trans.* **2016**, *45* (7), 2823−2828. (d) Denny, J. A.; Lamb, R. W.; Reilly, S. W.; Donnadieu, B.; Webster, C. E.; Hollis, T. K. Investigation of metallation/transmetallation reactions to synthesize a series of CCC−NHC Co pincer complexes and their X-ray structures. *Polyhedron* **2018**, *151*, 568−574. (e) Bauer, E. B.; Andavan, G. S.; Hollis, T. K.; Rubio, R. J.; Cho, J.; Kuchenbeiser, G. R.; Helgert, T. R.; Letko, C. S.; Tham, F. S. Air- and Water-Stable Catalysts for Hydroamination/Cyclization. Synthesis and Application of CCC− NHC Pincer Complexes of Rh and Ir. *Org. Lett.* **2008**, *10* (6), 1175−1178. (f) Reilly, S. W.; Akurathi, G.; Box, H. K.; Valle, H. U.; Hollis, T. K.; Webster, C. E. β-Boration of α, β-unsaturated carbonyl compounds in ethanol and methanol catalyzed by CCC-NHC pincer Rh complexes. *J. Organomet. Chem.* **2016**, *802*, 32−38. (g) Denny, J. A.; Lang, G. M.; Hollis, T. K. CCC-NHC pincer complexes: synthesis, applications, and catalysis. In *Pincer Compounds*; Elsevier, 2018; pp 251−272. (h) Zhang, X.; Cao, B.; Valente, E. J.; Hollis, T. K. Synthesis, characterization, photoluminescence, and simulations of a CCC-NHC-supported Pt2Ag2 mixed-metal cluster containing a PtAg2 metallacyclopropane. *Organometallics* **2013**, *32* (3), 752−761. (i) Vargas, V. C.; Rubio, R. J.; Hollis, T. K.; Salcido, M. E. Efficient route to 1, 3-Di-N-imidazolylbenzene. A comparison of monodentate vs bidentate carbenes in Pd-catalyzed cross coupling. *Org. Lett.* **2003**, *5* (25), 4847−4849.
(48) (a) Moulton, C. J.; Shaw, B. L. Transition metal−carbon bonds. Part XLII. Complexes of nickel, palladium, platinum, rhodium and iridium with the tridentate ligand 2, 6-bis [(di-t-butylphosphino) methyl] phenyl. *J. Chem. Soc., Dalton Trans.* **1976**, No. 11, 1020−1024. (b) Van der Boom, M. E.; Milstein, D. Cyclometalated phosphine-based pincer complexes: mechanistic insight in catalysis, coordination, and bond activation. *Chem. Rev.* **2003**, *103* (5), 1759−1792. (c) Gupta, M.; Hagen, C.; Flesher, R. J.; Kaska, W. C.; Jensen, C. M. A highly active alkane dehydrogenation catalyst: stabilization of dihydrido rhodium and iridium complexes by a P−C−P pincer ligand. *Chem. Commun.* **1996**, *17*, 2083−2084. (d) Park, D.-A.; Byun, S.; Ryu, J. Y.; Lee, J.; Lee, J.; Hong, S. Abnormal N-Heterocyclic Carbene−Palladium Complexes for the Copolymerization of Ethylene and Polar Monomers. *ACS Catal.* **2020**, *10* (10), 5443−5453.
(49) (a) Marelius, D. C.; Darrow, E. H.; Moore, C. E.; Golen, J. A.; Rheingold, A. L.; Grotjahn, D. B. Hydrogen-Bonding Pincer Complexes with Two Protic N-Heterocyclic Carbenes from Direct Metalation of a 1, 8-Bis (imidazol-1-yl) carbazole by Platinum, Palladium, and Nickel. *Chemistry−A European Journal* **2015**, *21* (31), 10988−10992. (b) Zou, T.; Lok, C.-N.; Wan, P.-K.; Zhang, Z.-F.; Fung, S.-K.; Che, C.-M. Anticancer metal-N-heterocyclic carbene complexes of gold, platinum and palladium. *Curr. Opin. Chem. Biol.* **2018**, *43*, 30−36. (c) Therrien, J.; Wolf, M.; Patrick, B. Synthesis and comparison of nickel, palladium, and platinum bis (N-heterocyclic carbene) pincer complexes for electrocatalytic CO 2 reduction. *Dalton Trans.* **2018**, *47* (6), 1827−1840. (d) Taakili, R.; Barthes, C.; Goëffon, A.; Lepetit, C.; Duhayon, C.; Valyaev, D. A.; Canac, Y. NHC core phosphonium ylide-based palladium (II) pincer complexes: the second ylide extremity makes the difference. *Inorg. Chem.* **2020**, *59* (10), 7082−7096. (e) Yan, J.; Wang, Y.-B.; Zhu, Z.-H.; Li, Y.; Zhu, X.; Hao, X.-Q.; Song, M.-P. Synthesis, Characterization, and Catalytic Studies of Unsymmetrical Chiral NCC Pincer Pd (II) and Ni (II) Complexes Bearing (Imidazolinyl) aryl NHC Ligands. *Organometallics* **2018**, *37* (14), 2325−2334.
(50) Huckaba, A. J.; Cao, B.; Hollis, T. K.; Valle, H. U.; Kelly, J. T.; Hammer, N. I.; Oliver, A. G.; Webster, C. E. Platinum CCC-NHC benzimidazolyl pincer complexes: synthesis, characterization, photostability, and theoretical investigation of a blue-green emitter. *Dalton Trans.* **2013**, *42* (24), 8820−8826.
(51) (a) Helgert, T. R.; Hollis, T. K.; Valente, E. J. Synthesis of titanium CCC-NHC pincer complexes and catalytic hydroamination of unactivated alkenes. *Organometallics* **2012**, *31* (8), 3002−3009. (b) Lee, C.-S.; Sabiah, S.; Wang, J.-C.; Hwang, W.-S.; Lin, I. J. B. Water-Induced Changes of Photoluminescence of a Pincer-Type N-Heterocyclic Carbene Platinum(II) Complex. *Organometallics* **2010**, *29* (2), 286−289.
(52) Zhang, X.; Wright, A. M.; DeYonker, N. J.; Hollis, T. K.; Hammer, N. I.; Webster, C. E.; Valente, E. J. Synthesis, Air Stability, Photobleaching, and DFT Modeling of Blue Light Emitting Platinum CCC-N-Heterocyclic Carbene Pincer Complexes. *Organometallics* **2012**, *31* (5), 1664−1672.
(53) (a) Creech, J.; Baker, J.; Handler, M.; Bizzarro, M. Platinum stable isotope analysis of geological standard reference materials by double-spike MC-ICPMS. *Chem. Geol.* **2014**, *363*, 293−300. (b) Hunt, A. C.; Ek, M.; Schönbächler, M. Separation of Platinum from Palladium and Iridium in Iron Meteorites and Accurate High-Precision Determination of Platinum Isotopes by Multi-Collector ICP-MS. *Geostand. Geoanal. Res.* **2017**, *41* (4), 633−647.
(54) Compain, G.; Sikk, L.; Massi, L.; Gal, J. F.; Duñach, E. Bond strength and reactivity scales for Lewis superacid adducts: a comparative study with In (OTf) 3 and Al (OTf) 3. *ChemPhysChem* **2017**, *18* (6), 683−691.
(55) Adamo, C.; Barone, V. Toward reliable density functional methods without adjustable parameters: The PBE0 model. *J. Chem. Phys.* **1999**, *110* (13), 6158−6170.
(56) Grimme, S.; Antony, J.; Ehrlich, S.; Krieg, H. A consistent and accurate ab initio parametrization of density functional dispersion correction (DFT-D) for the 94 elements H-Pu. *J. Chem. Phys.* **2010**, *132* (15), 154104.
(57) (a) Wadt, W. R.; Hay, P. J. Ab initio effective core potentials for molecular calculations. Potentials for main group elements Na to Bi. *J. Chem. Phys.* **1985**, *82* (1), 284−298. (b) Hay, P. J.; Wadt, W. R. Ab initio effective core potentials for molecular calculations. Potentials for K to Au including the outermost core orbitals. *J. Chem. Phys.* **1985**, *82* (1), 299−310.
(58) Marenich, A. V.; Cramer, C. J.; Truhlar, D. G. Universal Solvation Model Based on Solute Electron Density and on a

https://doi.org/10.1021/acs.organomet.3c00411
Organometallics XXXX, XXX, XXX−XXX

Continuum Model of the Solvent Defined by the Bulk Dielectric Constant and Atomic Surface Tensions. *J. Phys. Chem. B* **2009**, *113* (18), 6378−6396.

(59) (a) Wennmohs, F.; Neese, F. A comparative study of single reference correlation methods of the coupled-pair type. *Chem. Phys.* **2008**, *343* (2), 217−230. (b) Neese, F.; Valeev, E. F. Revisiting the Atomic Natural Orbital Approach for Basis Sets: Robust Systematic Basis Sets for Explicitly Correlated and Conventional Correlated ab initio Methods? *J. Chem. Theory Comput.* **2011**, *7* (1), 33−43. (c) Sandhoefer, B.; Kossmann, S.; Neese, F. Derivation and assessment of relativistic hyperfine-coupling tensors on the basis of orbital-optimized second-order Møller−Plesset perturbation theory and the second-order Douglas−Kroll−Hess transformation. *J. Chem. Phys.* **2013**, *138* (10), 104102.

(60) Neese, F.; Wennmohs, F.; Becker, U.; Riplinger, C. The ORCA quantum chemistry program package. *J. Chem. Phys.* **2020**, *152* (22), 224108.

(61) Rappoport, D.; Furche, F. Property-optimized Gaussian basis sets for molecular response calculations. *J. Chem. Phys.* **2010**, *133* (13), 134105.

https://doi.org/10.1021/acs.organomet.3c00411
Organometallics XXXX, XXX, XXX−XXX